MODELING CRACKS IN NONLINEAR VISCOELASTIC MEDIA SUBJECTED TO THERMAL LOADING

by

Çağrı İyidiker

B.S., Mechanical Engineering Department, Boğaziçi University, 2008

Submitted to the Institute for Graduate Studies in
Science and Engineering in partial fulfillment of
the requirements for the degree of
Master of Science

Graduate Program in Mechanical Engineering
Boğaziçi University
2014

ACKNOWLEDGEMENTS

I would like to express my sincere gratitude to my advisor Assoc. Prof. Şebnem Özüpek for useful comments, remarks and encouragement through the learning process of M.S Thesis study. I am also grateful to Mr. Namık Kılıç for tolerating me to go to the classes in busy work days and for his continuous support. He never complained about my frequent absence. Furthermore special thanks are given to OTOKAR Automotive and Defence Industry co. which I have been working for 5 years, every second of which is full of knowledge and experience.

And...

I would like to thank my wife Funda who is always respectful to my studies and would like to thank my parents not for a particular reason but for everything they have done for me.

ABSTRACT

MODELING CRACKS IN NONLINEAR VISCOELASTIC MEDIA SUBJECTED TO THERMAL LOADING

This thesis study deals with the crack initiation and propagation analyses in finitely deforming viscoelastic media. The main goal of the study is to obtain a methodology for crack propagation analyses in bulk material and interface debonding using Extended Finite Elements (XFEM) and Cohesive Zone Modeling (CZM). Firstly several benchmark analyses were performed using CZM, XFEM and conventional crack propagation method based on J integral and the results were evaluated. Then using an analog rocket motor from literature, stress analyses were performed for bore cracking and debonding under monotonic temperature loading. The results were compared qualitatively and quantitatively with the test results of related studies from literature to verify the model to be used for propagation analyses. Finally, crack propagation was analyzed under cyclic temperature loadings for several initial defect sizes and crack growth was calculated as a function of loading. It is concluded that, XFEM and CZM are efficient and appropriate methods for crack propagation analysis in nonlinear viscoelastic media.

ÖZET

ISIL YÜKLEMEYE MARUZ KALAN DOĞRUSAL OLMAYAN VİSKOELASTİK ORTAMLARDA ÇATLAK MODELLEMESİ

Bu tez çalışması sonlu şekil değişimi gösteren viskoelastik ortamlardaki çatlak başlangıcı ve çatlak ilerlemesi analizlerini konu almaktadır. Çalışmanın temel amacı Extended Finite Elements (XFEM) ve Cohesive Zone Model (CZM) yöntemini kullanarak malzemedeki çatlak ilerlemesi ve arayüzeydeki ayrılma analizleri için bir metodoloji geliştirmektedir. İlk önce CZM, XFEM ve J ingegral tabanlı konvansiyonel yöntem kullanılarak bazı karşılaştırmalı değerlendirme (benchmark) çalışmaları gerçekleştirildi. Daha sonra literatürden alınan katı yakıtlı analog roket motorunda yakıt iç yüzeyinde çatlak ve arayüzeyde ayrılma durumları için soğuma ısıl yüklemesi altında gerilme analizleri gerçekleştirildi. Öngörülerin literatürdeki sonuçlarla nicel ve nitel olarak karşılaştırılması yapılarak çatlak ilerleme analizinde kullanılacak model doğrulandı. Son olarak çevrimsel sıcaklık yüklemesi altında çeşitli başlangıç çatlak boyları için çatlak analizleri gerçekleştirildi ve çatlak ilerlemesinin yükleme ile değişimi hesaplandı. Analizlerin sonunda, XFEM ve CZM' nin doğrusal olmayan viskoelastic ortamlardaki çatlak ilerleme analizleri için etkin ve pratik yöntemler olduğu sonucuna varıldı.

TABLE OF CONTENTS

ACKNOWLEDGEMENTS . . . iii
ABSTRACT . . . iv
ÖZET . . . v
LIST OF FIGURES . . . ix
LIST OF TABLES . . . xiv
LIST OF SYMBOLS . . . xv
LIST OF ACRONYMS/ABBREVIATIONS . . . xvii
1. INTRODUCTION . . . 1
1.1. Objectives of the Study . . . 6
2. BENCHMARK STUDIES . . . 8
2.1. An Introduction to Benchmark Studies . . . 8
2.1.1. Standard Method Based on Contour Integral Evaluation . . . 8
2.1.2. Cohesive Zone Modeling . . . 9
2.1.3. Extended Finite Element Method (XFEM) . . . 11
2.2. Benchmark Study 1 . . . 13
2.2.1. Problem . . . 13
2.2.1.1. Material Model . . . 14
2.2.1.2. Boundary Conditions and Loading . . . 14
2.2.1.3. Damage Parameters . . . 14
2.2.2. Finite Element Analysis Results . . . 15
2.2.2.1. Standard Method Using J Integral . . . 15
2.2.2.2. XFEM Solution with LEFM . . . 15
2.2.2.3. XFEM Solution with Traction - Separation . . . 17
2.2.2.4. Solution with CZM . . . 17
2.2.2.5. Evaluation of Results . . . 18
2.3. Benchmark Study 2 . . . 19
2.3.1. Problem . . . 20
2.3.1.1. Material Model . . . 20
2.3.1.2. Boundary Conditions and Loading . . . 20

2.3.1.3. Damage Parameters 22
2.3.2. Finite Element Analysis Results 22
2.4. Benchmark Study Conclusions 23
3. BORE CRACK 25
3.1. Problem Description 25
3.2. Geometry 25
3.3. Material Models 26
3.3.1. Nonlinear Viscoelastic Material Properties 26
3.3.2. Damage Model for Crack 28
3.4. Effects of Bore Crack on Stress Distribution 28
3.4.1. Finite Element Model 29
3.4.1.1. Boundary Conditions and Loading 29
3.4.1.2. Mesh Convergence 29
3.4.2. Finite Element Analysis Results 30
3.4.2.1. Radial Stress Change 31
3.4.2.2. Uni-axial Tension Test 34
3.4.2.3. Cyclic Temperature Loading 34
3.5. Bore Crack Propagation 37
3.5.1. Finite Element Model 37
3.5.1.1. Boundary Conditions and Loading 37
3.5.2. Using XFEM in Bore Crack Problem 38
3.5.2.1. Element Size 38
3.5.3. Finite Element Analysis Results 39
3.5.3.1. Cooling from 60 C to -40 C 40
3.5.3.2. J Integral Solution for 4mm Initial Crack Size 40
3.5.3.3. Cyclic Loading 43
4. DEBONDING 46
4.1. Effects of Debonding on Bond Stress Distribution 46
4.1.1. Finite Element Model 47
4.1.1.1. Material Model 47
4.1.1.2. Boundary Conditions and Loading 49
4.1.2. Finite Element Analysis Results 49

4.1.2.1. Effect of Nonlinearity in Bond-stress 49
4.1.2.2. Effect of Viscoelasticity 51
4.2. Crack Propagation for Debonding 52
4.2.1. Finite Element Model 54
4.2.1.1. Boundary Conditions and Loading 54
4.2.2. Using CZM in Debonding Problem 55
4.2.2.1. Damage Model 56
4.2.3. Finite Element Analysis Results 56
4.2.3.1. Cooling from 60 °C to -40 °C 56
4.2.3.2. Cyclic Loading 58
4.2.4. Debonding Study Conclusions 60
5. CONCLUSION 61
REFERENCES 65

LIST OF FIGURES

Figure 2.1. Flat surfaced notch in two dimensional deformation field. Γ is any curve surrounding the notch tip, Γ_1 denotes the curved notch tip [1]. 9

Figure 2.2. Schematic representation of cohesive zone at the crack tip [2,3]. . 10

Figure 2.3. (a) Linear and (b) non-linear traction separation model. 12

Figure 2.4. Benchmark geometry. 13

Figure 2.5. Benchmark FE model. 14

Figure 2.6. Comparison of J integral values and total strain energy with increasing crack length. 16

Figure 2.7. Time vs. Crack size (Conventional J Integral Method). 16

Figure 2.8. Applied displacement vs. Crack length (XFEM w/ LEFM). 17

Figure 2.9. Applied displacement vs. Crack length (XFEM w/ Traction - Separation). 18

Figure 2.10. Applied displacement vs. Crack length (CZM Solution). 18

Figure 2.11. Plots of crack propagation histories for the four methods. 20

Figure 2.12. Benchmark geometry and boundary conditions [4]. 21

Figure 2.13. Comparison of von mises stress contours and deformation shapes of XFEM and the results taken from the literature [4]. 22

Figure 2.14. Reaction force vs. time: comparison of analysis results with the reference. 23

Figure 3.1. Analogue motor geometry for crack propagaiton analysis (ϕ: diameter). 25

Figure 3.2. Traction - Separation curve of the propellant [4]. 28

Figure 3.3. Finite element mesh for the bore crack analysis. 29

Figure 3.4. Mesh convergence plot. 30

Figure 3.5. Location of sensors (a); Radial stress distribution along bond line for 5mm crack case (b) [5]. 31

Figure 3.6. Radial stress distribution along bond line (current study). 32

Figure 3.7. Crack length vs. bond stress. 33

Figure 3.8. Contour plot of S11 for 32mm crack. 33

Figure 3.9. Contour plot of S22 for 32mm crack. 34

Figure 3.10. Material responses for uniaxial tension at constant strain rate of $0.7291 min^{-1}$ [5]. 35

Figure 3.11. Measured temperature profile and the measured bond stresses during mechanical aging test of the motor [5]. 35

Figure 3.12. The temperature profile of the FEA. 36

Figure 3.13. Bond stress history of the current study. 36

Figure 3.14. Analysis model. 38

Figure 3.15. Cyclic temperature loading. 38

Figure 3.16. Loading profile for sensitivity analysis. 39

Figure 3.17. Crack propagation history for two different element sizes. 40

Figure 3.18. Crack propagation histories for various initial crack lengths. 41

Figure 3.19. Increase in the crack size vs. initial crack size. 41

Figure 3.20. Circumferential stress distribution for various crack growth analyses (time t = 780 minutes). 42

Figure 3.21. Representation of the cohesive zone. 42

Figure 3.22. Energy dissipation resulting from XFEM solution. 43

Figure 3.23. J integrals for 4mm and 6mm stationary crack analysis. 44

Figure 3.24. Circumferential stress change at the crack tip during the cyclic loading (4mm initial crack case). 45

Figure 4.1. The analogue motor geometry [6]. 47

Figure 4.2. Finite Elements Mesh model. 47

Figure 4.3. Stress - Strain curves as a result of uniaxial tension analyses for different material models. 48

Figure 4.4. Radial Stress Distribution at -40 C of 20 deg debonding case of Referenced study [6] and the current study. 50

Figure 4.5. Stress change along the bond line for the linear elastic material model of the referenced study (left) and current study (right). . . 50

Figure 4.6. Radial stress changes along the bond for linear elastic and nonlinear elastic cases. 51

Figure 4.7. Percent stress drops for linear elastic, nonlinear elastic and nonlinear viscoelastic material types. 52

Figure 4.8. Radial stress changes along the bond for nonlinear elastic and nonlinear viscoelastic cases. 53

Figure 4.9. Analysis model. 54

Figure 4.10. Analysis model. 55

Figure 4.11. Traction - Separation curve of the propellant. 56

Figure 4.12. Crack size vs. Time plot. 57

Figure 4.13. Enriched regions along the bond-line. 57

Figure 4.14. Increase in the crack size vs. initial crack size. 58

Figure 4.15. Final states of the propagation. 59

Figure 4.16. Representation of the cohesive zone. 59

Figure 4.17. Stress history during the cyclic loading (15 deg initial debonding case). 60

LIST OF TABLES

Table 2.1. Damage parameters for traction - separation model. 15

Table 2.2. Crack propagation histories for the three methods. 19

Table 2.3. Benchmark linear viscoelastic material model ($E_0 = 20MPa$) [4]. . 21

Table 2.4. Damage parameters for crack propagation [4]. 22

Table 3.1. FRP case material properties [7]. 26

Table 3.2. Normalized Prony series for NLVE material [7]. 27

Table 3.3. Maximum stress drop along bond-line for different bore crack sizes. 32

Table 3.4. Peak stresses corresponding to loading cycles in Figure 3.12. 37

Table 4.1. Radial stresses for various cases (Linear elastic: [6] and Nonlinear elastic: Current Study). 51

Table 4.2. Tabular representation of stress drops for the debonding cases (Non-Linear elastic and Nonlinear Viscoelastic). 53

LIST OF SYMBOLS

a	Initial crack size of benchmark specimen
B	Thickness of benchmark specimen
E	Elastic modulus
E_i	Relaxation modulus terms of prony series
G^c	Fracture energy of propellant
G_0	Instantaneous shear modulus
g_i^P	Relaxation shear modulus of prony series
G_∞	The equilibrium shear modulus
H	Height of benchmark specimen
I_1	First deviatoric strain invariant
J	J integral
J^{el}	Elastic volume ratio
J_{Ic}	Critical J integral
K_{nn}	Stiffness in normal direction
K_{ss}	Stiffness in shear direction
K_{tt}	Stiffness in tangential direction
P	Total potential energy of cracked body
s11	Radial stress
s22	Tangential stress
t_c	Maximum traction of propellant
u	Displacement
w	Width of benchmark specimen
$W(x_1, x_2)$	Strain energy density
α	Thermal expansion coefficient
α_{pro}	Thermal expansion coefficient of propellant
Δa	size of crack propagation
Δu	Change in the total energy of the structure
θ_0	Stress free temperature of propellant

ν	Poisons ratio
σ_{jk}	Stress tensor
τ_i	Time variable of prony series
τ_i^G	Time variable of prony series

LIST OF ACRONYMS/ABBREVIATIONS

CAE	Complete Abaqus Environment
CPE4	4 Noded Continuum Plain Strain Element
CZM	Cohesive Zone Model
DCB	Double Cantilever Beam
FE	Finite Elements
FEM	Finite Elements Method
FRP	Fiber Reinforced Plastics
HTPB	Hydroxyl-Terminated PolyButadiene
LEFM	Linear Elastic Fracture Mechanics
LVE	Linear ViscoElastic
NLVE	NonLinear ViscoElastic
SIF	Stress Intensity Factor
SRM	Solid Rocket Motor
XFEM	Extended Finite Elements Method

1. INTRODUCTION

Crack propagation studies have always been an important part of engineering problems since the majority of failures in machinery is due to a sudden propagation of an existing crack or propagation of micro cracks due to high cycle fatigue. While the later one is important for durability issues and can be foreseen before final failure using various fatigue theories like Miner's rule [8], the former one is important in order not to cause any catastrophe or functionality problems since it may occur all in a sudden. Therefore, crack initiation and crack growth predictions are important but equally difficult parts of failure analysis. The main objectives of crack analyses are to detect potential crack initiations to foresee the path of possible propagation and to determine the speed of the propagation. These parameters are important for deciding the service life of a component and taking precautions before failure.

Conventional Crack propagation analyses are mostly based on stress intensity factor or J integral approach [9–14]. Stress intensity factor is defined for a linear material and its critical value is called fracture toughness. It is specific to the material and is related to the energy needed for crack growth. The main principle underlying fracture toughness based crack analysis is that when the stress intensity factor (SIF) exceeds a critical value, then the crack starts to propagate. Beside stress intensity factor, another important quantity for crack analysis is the J integral value. J integral is a path independent integral which can be used like stress intensity factor [1] and contrary to SIF approach, J integral can also be used for nonlinear materials. J integral is equivalent to the amount of energy needed to generate unit area of crack surface [12]. Critical J values for growing cracks are obtained in laboratory environment following some of the standardized experimental procedures, such as ASTM E1820 [14, 15]. In addition to these test methods, there are many applications in the literature dealing with the calculation of J integral based on Finite Elements Method (FEM) [9, 12, 13]. Although FEM make the calculation of stress intensity factors and J integral easier, propagation analysis with conventional methods are still cumbersome for complex geometries since determining the path of the propagation is computationally expensive.

The particular problem of interest in this study is the simulation of crack initiation and crack growth in solid rocket motors subjected to thermal loading. Challenges associated with this problem are discussed below along with some literature review.

A useful and relatively new method related to crack propagation in rocket motors is a test based crack monitoring system also called as health monitoring systems [16,17]. In health monitoring systems the defects in the motor are detected based on bond stress measurements along the bondline. There are many studies dealing with the simulation of these monitoring techniques based on FEM procedures [6,18–20]. Anhduong *et al.* [6] applied the finite element method to investigate the effect of delamination on the radial stress distribution at the bondline during the cooling process of a solid rocket motor consisting of propellant, insulation, and casing. A relationship is established among the debond angle, the number of sensors, and the required sensor accuracy. According to the study, increasing the number of sensors improves the detectability, however this also increases the cost and the complexity of the health monitoring system.

Another study [20] deals with the experimental investigation of the effect of defects on the radial stress distribution along the circumference. Similar to [6], a cooling process is applied to the rocket motor and changes in the radial stress reading of the sensors are observed. The process is also simulated using commercially available FEM software ABAQUS. At the end of the study, the bond stress sensors have proven to be very valuable for gaining better understanding of the stresses and especially the mechanical ageing of a solid propellant rocket motor. One drawback of this study is that, in the FEM part of the study, linear viscoelastic (LVE) propellant material is used.

A similar work on health monitoring systems is the study performed by Miller *et al.* [18]. In this study, similar to the above studies, stress transducers are mounted between the case wall and the propellant in order to monitor the debondings. This study concludes that with the number and sensitivity of sensors, the location and size of the crack, and the type and magnitude of the applied load, all affect the overall system capability.

The above studies are significant for detecting the existing cracks in SRMs but they do not address the propagation of the present cracks. The crack propagation analysis of SRMs, which is the subject matter of the current thesis study, has various challenges associated with it. In the following a review of previous studies concerned with these challenges is presented.

LEFM models are not directly appropriate to SRM like structures due to viscoelasticity effects. Ho *et al.* [21] modified the classical formulation of LEFM and developed a method that accounts for bulk inelastic behaviour in the calculation of a critical strain energy release rate. The method is sufficiently accurate in predicting the thermal stresses in an end-burning rocket motor. Reasonably good agreement between the stresses measured using miniature normal stress sensors embedded in the propellant grain and the predicted von Mises stresses were obtained. However, the effect of previous loading histories and, therefore, possible damage in the material,on the relaxation modulus have been neglected in the study.

Liu [22] studied the local behavior near the crack tip and the crack growth behavior in a composite solid propellant under various loading conditions and revealed the effect of these conditions on several factors. Experimental results indicate that the time-dependent damage process is a contributing factor to the time-dependent fracture behavior near the crack tip. He also indicates that the near tip mechanisms (blunting, voiding, coalescing and growing) are the same over the range of test conditions, differing only in a quantitative sense.

Schapery developed a method [23] for predicting the time-dependent size and shape of cracks in linearly viscoelastic, isotropic media, and demonstrated by applying the theory to crack growth end failure of unfilled and particulate filled polymers. The study of Rao [24] presents relevant information for the development of a fracture criterion for solid propellant grains. Determination of the crack tip stress intensity factor, evaluation of fracture toughness and establishment of the crack growth rate equation through fracture properties are discussed.

In William's study [21], the work of Griffith on crack initiation is extended analytically to linear viscoelastic materials using thermodynamic approach. Then formulation is used with a cyclic sinusoidal loading to see if the nature of the theoretical predictions seems to be in accordance with expectations. Although correlation is established with the expectations, the resulting model has to be tested with experimental results for practical situations.

Alternative technique which can be used for the crack propagation analysis of non-linear viscoelastic propellants is the cohesive zone model (CZM). Cohesive zone of a crack is the portion of the crack in which the crack is initiated but the crack faces are not fully separated. Pioneering works in CZM are due to Needleman and his co-workers [25, 26], and Camacho and Ortiz [27]. Xu and Needleman [26] proposed a potential-based cohesive zone model in which cohesive elements are inserted into a finite element mesh [2].

The name CZM mostly stands for the damage model called traction-separation law which represents the fracture process zone [4]. In crack propagation procedure based on CZM the separation of two bonded faces is managed by traction-separation properties of the adhesive material or the bonded interface.

CZM is a good method for separation analysis of bonded surfaces. One potential use of this procedure that could compromise the reliability and long-term durability is in solid rocket motors where the bond-line is quite a complex system that involves layers of primer, adhesive, insulator and liner between the case and propellant. CZM can reduce this system to a single traction-separation curve between two faces. Liechti et al [28] investigated a rate-dependent traction-separation law for modelling quasi-static debonding between propellant and the case. In this study, the traction-separation law were extracted on the basis of measurements of load, crack length and crack opening displacements in an opening mode experiment at one applied displacement rate.

Diehl [29] demonstrated the use of a penalty methodology for utilizing cohesive elements to simulate flexible and inelastic peal arm deformation problems. Accuracy

of the method is demonstrated by comparing simulation results to experimental data of epoxy bonded aluminum arms being peeled at different angles from a rigid substrate. This work addresses significant complexities in the analysis that arise due to the inelastic deformation of the aluminum peel arms.

Lucas *et al.* [29] used a cohesive model for fatigue crack initiation. Cohesive elements are placed at the boundary between adjacent standard volume finite elements to model fatigue damage that leads to fracture at the separation of the element boundaries per the cohesive law.

One major drawback of CZM in crack propagation problems is that the path of the propagation has to be known. Han et al. [4] used CZM in mixed mode crack propagation analysis of a double edge notched specimen. Since the crack direction and path are not predefined, cohesive elements are inserted to all surfaces between normal elements. This is computationally intensive, making CZM attractive mostly for predefined-path crack problems, such as that of interface debonding.

For undefined-path crack analysis, one of the most powerful analysis method is the Extended Finite Elements Method (XFEM). XFEM enables the accurate approximation of fields that involve jumps, kinks, singularities, and other non-smooth features within elements. This is achieved by adding additional terms—the enrichments—to classical finite element approximations. These terms enable the approximation to capture the non smooth features independently of the mesh [30].

XFEM can be used with LEFM and traction - separation models; predefined-path and undefined-path crack propagation analyses can be performed using XFEM. XFEM is not a common method for crack analysis of viscoelastic media. Toolabi *et al.* [31] used XFEM to analyse a 2-D cracked body made of a viscoelastic orthotropic material. The cracked body has a stationary edge crack and can be assumed a double cantilever beam (DCB). The method was used to capture modal stress intensity factors and the J-integral for viscoelasticity. The dynamic mixed mode stress intensity factors and the dynamic J-integral were compared with the results obtained from FEM and

a good correlation was established. In this study, however, only linear viscoelasticity was considered.

Zhang *et al.* [32] applied XFEM to solve crack problems in linear viscoelastic materials. Deformations such as crack opening and sliding displacements in a cracked viscoelastic body are numerically investigated by the XFEM. The solution is carried out directly in time domain with a mesh not conforming to the crack geometry. Numerical examples show that the crack opening displacement and crack sliding displacement are calculated satisfactorily. This study was carried out with linear viscoelastic materials. Nonlinearity was not taken into account.

1.1. Objectives of the Study

The main goal of this thesis study is to provide an efficient and appropriate analysis methodology for crack analyses of nonlinear viscoelastic media under temperature loading. First objective is to understand crack propagation analysis methods and procedures that can be performed within the finite element framework. The second objective is to apply XFEM and CZM to bore crack and debonding problems, respectively, in solid rocket motor. To this regard, firstly the effects of bore crack and debonding defects on the stress distribution along the bond line as a result of motor cooling are to be evaluated. Following this, crack growth analysis is performed, and a relation between the crack length and bond stress values is determined.

Although there are several mechanical loads the rocket motor is subjected to, such as pressurization during ignition, acceleration during storage and launch, the focus of this study is to consider loads that have the greatest effect on the service life, namely thermal loads.

The material model representing the propellant is a non-damaging nonlinear viscoelastic model. Although the most appropriate model for the propellant should include the damage evolving in the material as it is subjected to various loads, the study is mainly concerned with the exploration of computational techniques suitable for crack

analysis. The consequences of not accounting for damage are stated along with the discussion of results.

In Chapter 2, several benchmark analyses are presented. Sensitivities of XFEM and CZM are studied and the results are compared with the results of conventional method based on J Integral. In Chapter 3, stress analysis for stationary bore crack problem is presented and the results are compared with a related study from literature. In addition, crack propagation of a bore crack using XFEM with traction-separation damage model is described. In Chapter 4, the stress and propagation analysis for debonding case using CZM are performed. Conclusions and future work are presented in Chapter 5.

2. BENCHMARK STUDIES

2.1. An Introduction to Benchmark Studies

In this section, a brief summary of crack propagation methods that are considered in this study is given. The application of the methods within the finite element framework is emphasized and the related literature survey is presented.

2.1.1. Standard Method Based on Contour Integral Evaluation

The standard finite element method for simulation of crack propagation is based on modeling the existence of a crack and its propagation trajectory. Various criteria can be used to determine growth of the crack. Linear elastic fracture mechanics, LEFM, approach defines crack growth in terms of critical stress intensity factor which is based on singular stress field at the crack tip. In nonlinear materials considerable mathematical difficulties accompany the determination of concentrated strain fields near notches and cracks. Therefore the criterion most widely used for crack growth of large deformation materials is the critical tearing energy criterion. For a nonlinear elastic material the tearing energy is equal to the reduction in strain energy per unit area of crack growth. It is also equivalent to Rice's J integral. Rice [1] applied deformation plasticity to the analysis of a crack in a nonlinear material and showed that the nonlinear energy release rate could be written as a path independent contour integral. The approach is first to identify a line integral which has the same value for all integration paths surrounding a class of notch tips in two-dimensional deformation fields of linear or nonlinear elastic materials. The choice of a near tip path directly relates the integral to the locally concentrated strain field. In that, the J-integral characterizes crack tip stress and strain in nonlinear materials and can be viewed as both an energy parameter and stress intensity parameter. J_{Ic}, the critical value of J-integral at the onset of ductile crack extension, is a material parameter which can be used to judge the toughness of elasto-plastic materials.

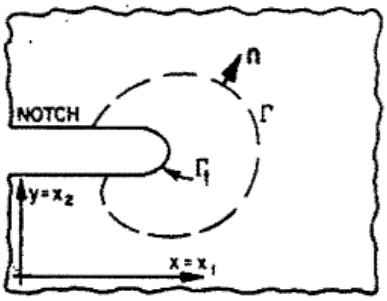

Figure 2.1. Flat surfaced notch in two dimensional deformation field. Γ is any curve surrounding the notch tip, Γ_1 denotes the curved notch tip [1].

The J-Integral around a crack tip is frequently expressed as

$$J := \int_{\Gamma} \left(W dx_2 - \mathbf{t}.\frac{\partial \mathbf{u}}{\partial x_1} ds \right) \tag{2.1}$$

where W(x_1,x_2) is the strain energy density, x_1,x_2 are the coordinate directions, $\boldsymbol{\sigma}$ is the Cauchy stress tensor, and $\mathbf{u}$ is the displacement vector. The strain energy density is given by

$$W = \int_0^{\epsilon} \boldsymbol{\sigma} : d\boldsymbol{\epsilon}; \tag{2.2}$$

In finite element analysis, the calculation of J-integral is a post-processing operation. In this study J-integral was evaluated in ABAQUS for various patches of elements surrounding the crack tip. The calculated value of J-integral was compared to the critical value of J to advance the crack.

2.1.2. Cohesive Zone Modeling

Cohesive zone modeling, CZM, offers an alternative approach to the LEFM. The latter assumes the existence of an infinitely sharp crack leading to singular crack tip fields. CZM assumes the existence of a fracture cohesive zone, called cohesive zone in which the crack is initiated but the crack faces are not fully separated. That is, the

compression force between the crack faces is not zero. The representation of cohesive zone is given in Figure 2.2. In this method the processes occurring within the cohesive zone are accounted for only through a traction-separation relation.

Cohesive zone modeling has gained considerable attention over the past decade, as it represents a powerful yet efficient technique for computational fracture studies. Although the early conceptual works related to the cohesive zone model (CZM) date back to the early 60s, during the 90s, leaps were made as a result of the pioneering works by Needleman and his co-workers [25, 26], and Camacho and Ortiz [27]. Xu and Needleman [26] proposed a potential-based cohesive zone model in which cohesive elements are inserted into a finite element mesh [2].

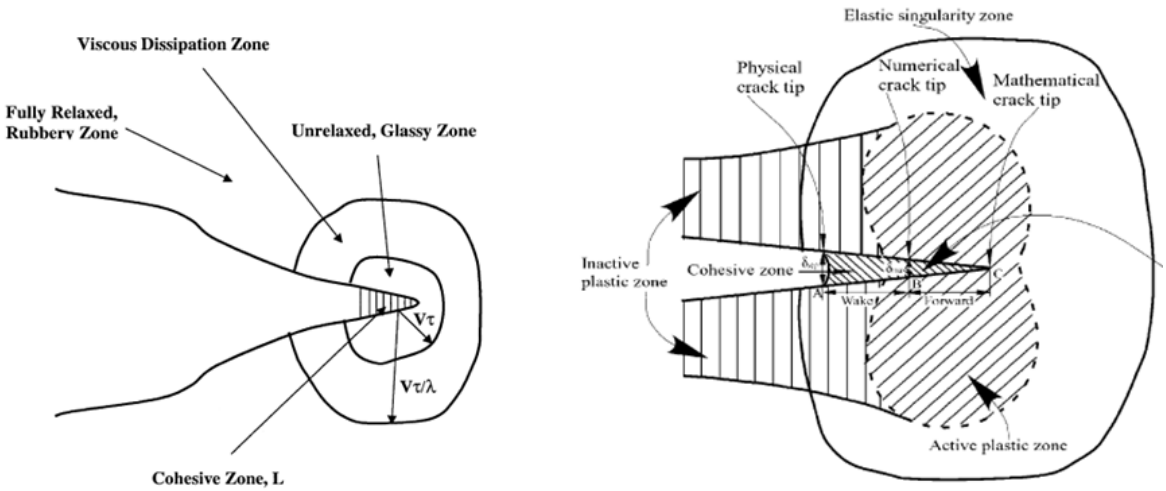

Figure 2.2. Schematic representation of cohesive zone at the crack tip [2, 3].

CZM has evolved as a preferred method to analyze fracture problems in monolithic and composite material systems not only because it avoids the singularity but also because it can be easily implemented in a numerical method of analysis as in finite element or boundary element method. CZMs have been used to simulate the fracture process in a number of material systems including polymers, metallic materials, etc [3].

In this study, we utilize the *surface based cohesive zone modeling* capability of

ABAQUS. In the classical chesive zone method, cohesive elements are used between the surfaces of crack path and crack propagation is simulated with separation of the nodes of these elements and deletion of these elements according to traction separation rule. In *surface based cohesive zone method*, however, upper and lower surfaces of the uncracked potions of crack path are glued together using bond contact property. The separation of these bonded surfaces is managed by traction-separation rule. The traction-separation model of ABAQUS consists of a stiffness matrix which relates the traction ($\mathbf{t}$) to the displacement ($\mathbf{u}$) at the crack tip.

$$\begin{bmatrix} t_n \\ t_s \\ t_t \end{bmatrix} = \begin{bmatrix} K_{nn} & & \\ & K_{ss} & \\ & & K_{tt} \end{bmatrix} \begin{bmatrix} d_n \\ d_s \\ d_t \end{bmatrix} \tag{2.3}$$

The terms K_{nn}, K_{ss}, K_{tt} are calculated based on the elastic properties for the cohesive section. Specifying the elastic properties of the material in an enriched region is sufficient to define both the elastic stiffness and the traction-separation behavior. For the latter initial behaviours is assumed to be linear elastic until the initiation of damage. The evolution of damage can be modeled as linear or nonlinear as shown in Figure 2.3.

In this study the CZM is to be explored for debonding at the interface between the case and the grain.

2.1.3. Extended Finite Element Method (XFEM)

The extended finite element method (XFEM) is developed to accurately approximate fields that involve jumps, kinks, singularities, and other non-smooth features within elements. This is achieved by adding terms, called the enrichments, to classical finite element approximations. These terms enable the approximation to capture the non smooth features independently of the mesh. The XFEM has shown its full potential for applications in fracture mechanics [33].

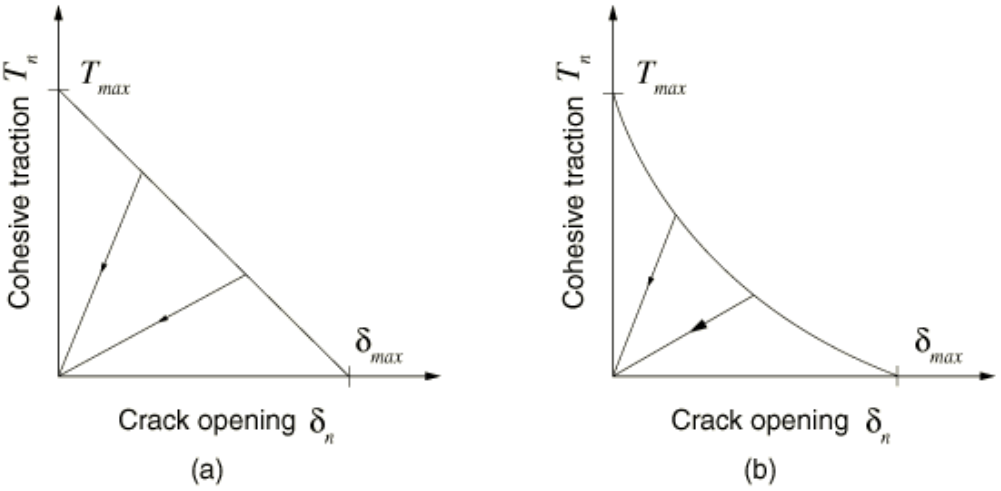

Figure 2.3. (a) Linear and (b) non-linear traction separation model.

Applications with cracks involve discontinuities across the crack surface and singularities (or general steep gradients) at the crack front in case of LEFM. In the standard FEM, a suitable mesh has to be provided and maintained which accounts for these features; this is particularly cumbersome for crack propagation in three dimensions. The XFEM, however, can treat these type of problems on fixed meshes and models crack propagation by a dynamic enrichment of the approximation. In other words, using XFEM has various advantages. First of which is that no initial crack is required. Once the crack initiates the path of the propagation does not need to be specified. The finte element code decides the direction of the crack growth according to the stress state at the crack tip. Another important advantage is that remeshing is not necessary for crack propagation analysis. Recent developments in the XFEM, are described in [34]; and an overview of the XFEM is given in Fries and Belytschko [35].

XFEM method can be used with both LEFM and cohesive zone (traction - separation) damage models. In benchmark problems analyzed in this thesis both methods are studied.

2.2. Benchmark Study 1

This benchmark problem deals with the study of crack propagation methods employing Extended Finite Element (XFEM), Cohesive Zone Method (CZM) and standard method using contour integral around the crack tip (J integral). For XFEM case, damage is modeled with two different ways: traction – separation method and linear elastic fracture mechanics method (LEFM).

2.2.1. Problem

Crack propagation of an edge crack in a linear elastic plate subjected to uniaxial tension is analyzed. The geometry shown in Figure 2.4 consists of 3m x 3m sheet with 0.3 m edge crack.

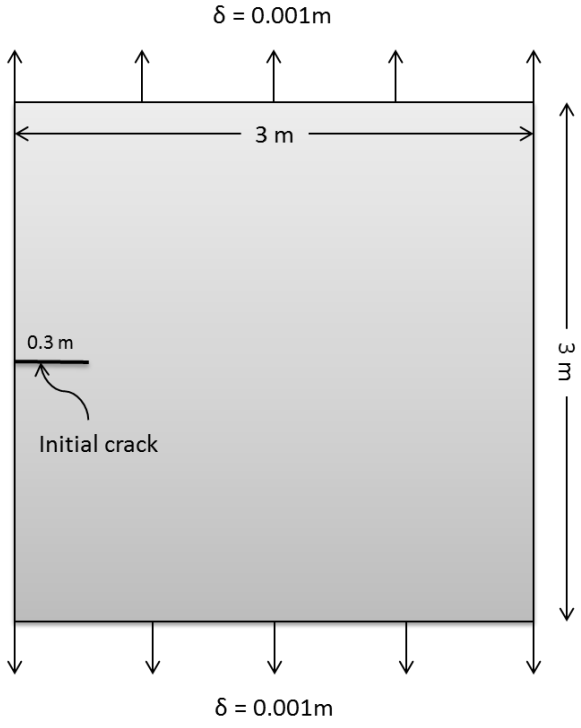

Figure 2.4. Benchmark geometry.

The finite element mesh consists of 1161 linear quadrilateral plane strain elements

(CPE4) as seen in Figure 2.5.

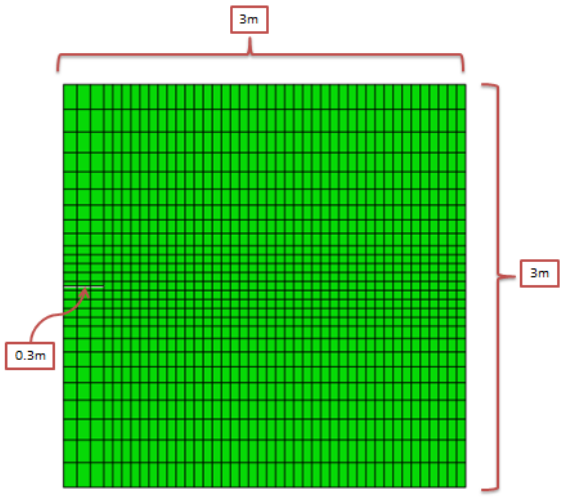

Figure 2.5. Benchmark FE model.

2.2.1.1. Material Model. The sheet material is steel modeled as linear elastic with Young's modulus of 210 GPa and Poisson ratio of 0.3.

2.2.1.2. Boundary Conditions and Loading. Uniaxial displacement of 0.001m is applied to the upper and the lower sides of the sheet. In this problem, symmetry boundary condition was not used since for XFEM, the crack propagates inside elements.

2.2.1.3. Damage Parameters. As mentioned above two different crack evolution models are used in this benchmark. The first one is the traction – separation model, the other is the LEFM. In both models, energy criterion is used for damage evolution. For traction – separation model, maximum stress criteria is used. The maximum stress and fracture energy parameters are given in Table 2.1.

Table 2.1. Damage parameters for traction - separation model.

Max Stress (MPa)	Critical Energy Release Rate (N/m)
220	42200

2.2.2. Finite Element Analysis Results

In this section crack propagation solutions using different techniques are presented and the results are evaluated.

2.2.2.1. Standard Method Using J Integral. In conventional method, for a given load and crack configuration, J integral value is calculated and compared to the critical value given in Table 2.1. When J reaches Jc, crack growth value Δa and growth direction are chosen and J integral value is again calculated for the new crack size (a + Δa). The J integral value gives the amount of energy needed to increase the crack by Δa for a unit thickness. Therefore, multiplying Δa by J value, we get the dissipated energy when the crack propagates with a length of Δa. That is, the change in total strain energy (ΔU) per crack elongation (Δa) and J integral have to be identical.

Figure 2.6 shows the comparison of J integral and ΔU/Δa. As can be seen, they are reasonably close for various crack sizes.

Figure 2.7 is the applied displacement vs. crack size graph obtained from crack propagation analysis with J integral approach. From Figure 2.7, propagation starts when the applied displacement is 0.00058m and total propagation of the crack is completed when the displacement is 0.00067m. From Figure 2.7, it can be concluded that after the propagation is initiated, the entire propagation occurs very quickly.

2.2.2.2. XFEM Solution with LEFM. The XFEM method is used with two different damage models. The first one is the linear elastic fracture mechanics (LEFM) model.

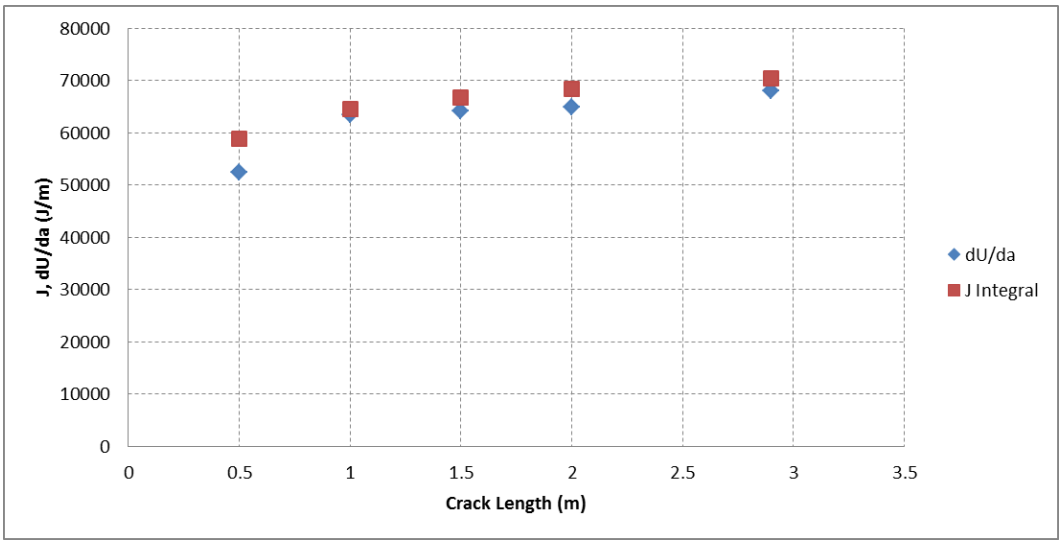

Figure 2.6. Comparison of J integral values and total strain energy with increasing crack length.

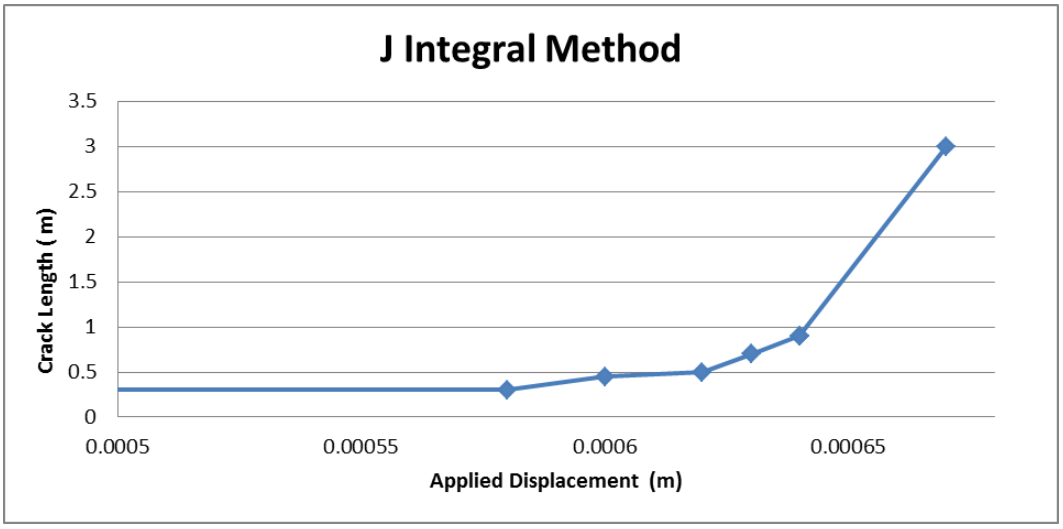

Figure 2.7. Time vs. Crack size (Conventional J Integral Method).

Figure 2.8 is the applied displacement vs. crack size graph of XFEM with LEFM method. In this method propagation starts when the applied displacement is 0.00052m and total propagation of the crack lasts when the applied displacement is 0.00065m as shown in Figure 2.8. That is, for LEFM based XFEM solution, the propagation of the crack initiates earlier than conventional method and thus total propagation is completed earlier.

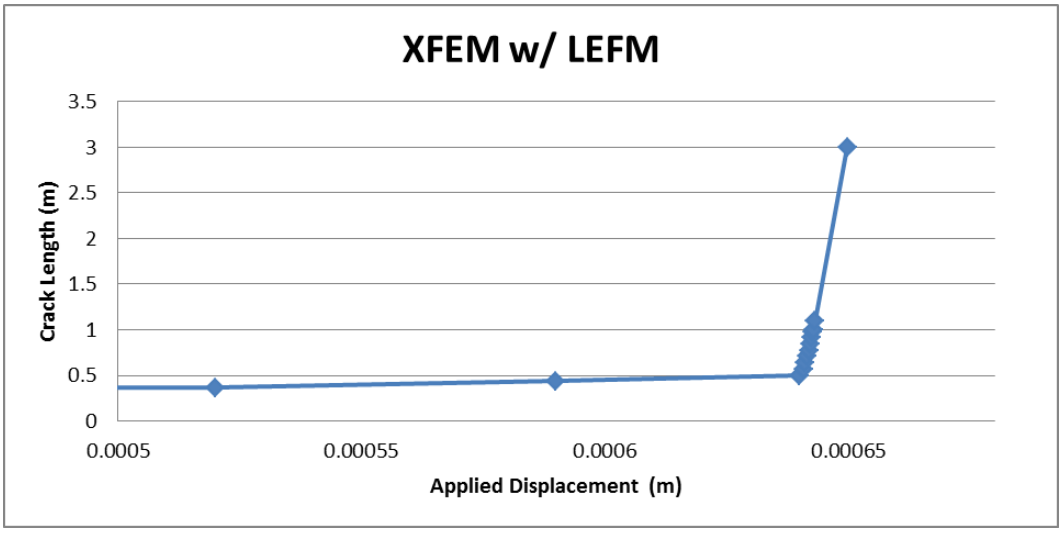

Figure 2.8. Applied displacement vs. Crack length (XFEM w/ LEFM).

2.2.2.3. XFEM Solution with Traction - Separation. In this analysis, XFEM is used with a traction separation damage model is used. As shown in Figure 2.9 the propagation starts when the applied displacement is 0.00059m and total propagation of the crack is completed when the applied displacement is 0.00065m. The crack propagation history of this method is very close to that of conventional method.

2.2.2.4. Solution with CZM. The cohesive zone method used in this study is surface based cohesive segment method of ABAQUS. This method is applied using bonded contact property of ABAQUS. The crack path is initially bonded. Cohesive and damage properties of the cohesive layer are defined for the contact region. Using this method propagation starts when the applied displacement is 0.00050m and total propagation

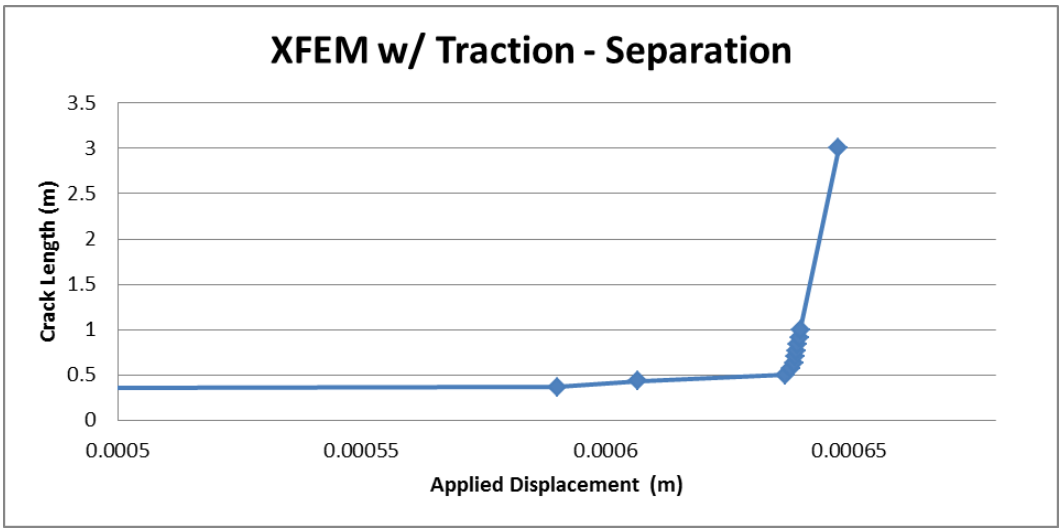

Figure 2.9. Applied displacement vs. Crack length (XFEM w/ Traction - Separation).

of the crack stops when the applied displacement is 0.00063m as shown in Figure 2.10. The propagation of the crack starts earliest among these four methods discussed here.

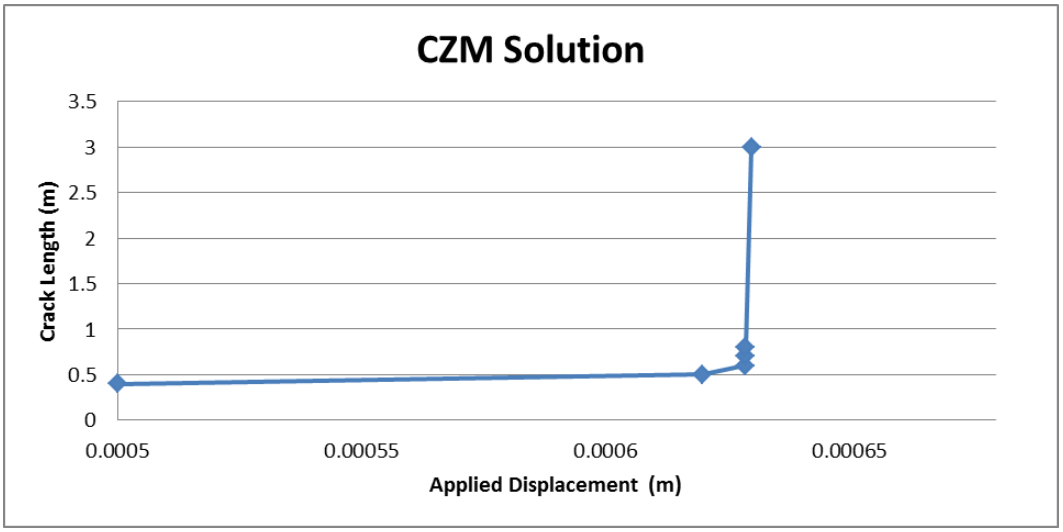

Figure 2.10. Applied displacement vs. Crack length (CZM Solution).

2.2.2.5. Evaluation of Results. Comparing the methods used for crack propagation analysis it is concluded that the history of the crack propagation profiles as a function

of applied displacements are similar for all of the methods except for slight differences in the initiation instants. When analysis procedure is XFEM, no matter if the damage model is traction-separation or LEFM, the results are very close to each other for the current problem. The most distinct results are for CZM and conventional method.

Since both the conventional and LEFM methods are similar in principle (That is, they use only energy principle), the results of the two methods are not too far to each other. The tabular and graphical comparisons of the results are shown in Figure 2.11 and Table 2.2. From the table, it can be seen that start and stop times of crack initiation and propagation are very close to each other. However, since the LEFM is known to be applicable to linear materials, for the rest of the analyses traction separation damage model will be used.

In order to evaluate the viscoelastic effects on the results the next benchmark study deals with the XFEM with traction – separation applied to linear viscoelastic media.

Table 2.2. Crack propagation histories for the four methods.

	Start of Propagation (m)	**End of Propagation (m)**
J Integral	0.00058	0.00067
XFEM w/ LEFM	0.00052	0.00065
XFEM w/ T- S	0.00059	0.00065
CZM	0.00050	0.00063

2.3. Benchmark Study 2

This benchmark study deals with the application of extended finite elements method to viscoelastic materials. The material model which is used in this study was taken from literature [4] and traction separation damage model was used in XFEM. The results obtained from the analysis are correlated with the reference test and analysis.

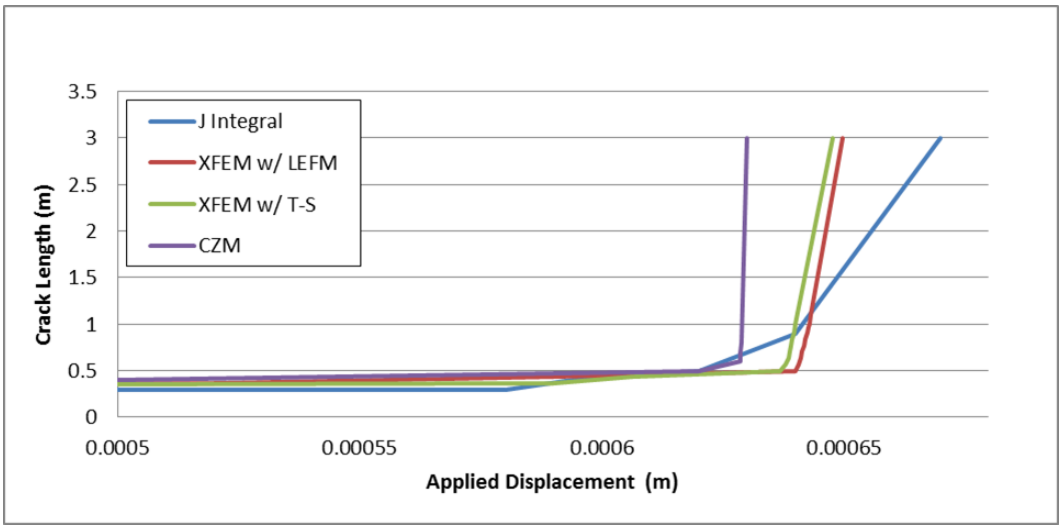

Figure 2.11. Plots of crack propagation histories for the four methods.

2.3.1. Problem

The benchmark model shown in Figure 2.12 is a double edge cracked specimen made of viscoelastic HTPB propellant material.

The model dimensions are W=30mm, H=70mm, B=5mm, a=10mm, d=20mm. The finite elements model is prepared using 2100 quadrilateral linear plane strain elements.

2.3.1.1. Material Model. The material of this problem is represented with a linear viscoelastic model. Relaxation modulus is represented with Prony Series as given in Table 2.3.

2.3.1.2. Boundary Conditions and Loading. The model is fixed at the bottom and pulled from the top with a rate of 20 mm/min. Boundary conditions are shown in Figure 2.12.

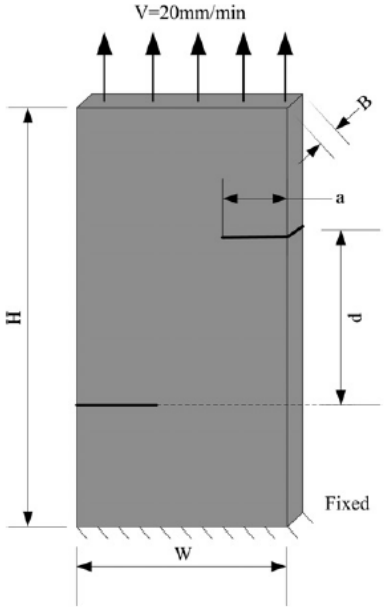

Figure 2.12. Benchmark geometry and boundary conditions [4].

Table 2.3. Benchmark linear viscoelastic material model ($E_0 = 20MPa$) [4].

i	$E_i(MPa)$	$\tau_i(s)$
1	8.37	0.592
2	1.80	1.148
3	1.56	12.081
4	0.734	55.579
5	0.431	217.588

2.3.1.3. Damage Parameters. The damage parameters for the problem were taken from the literature [4] which is an experimental study and are given in Table 2.4.

Table 2.4. Damage parameters for crack propagation [4].

Loading Rate (mm/min)	Fracture Energy (N/mm)	Strength (MPa)	Critical Separation Distance (mm)
20	1.007	0.548	3.22

2.3.2. Finite Element Analysis Results

This section contains the comparison of results obtained using XFEM method and the results of the literature [4].

Figure 2.13 shows Mises Stress contour plots of XFEM solution, CZM solution and the test result at time 27 sec. The plots of CZM solution and test result were taken from the literature [4]. As can be seen XFEM analysis is in a good correlation with the CZM result and the test result.

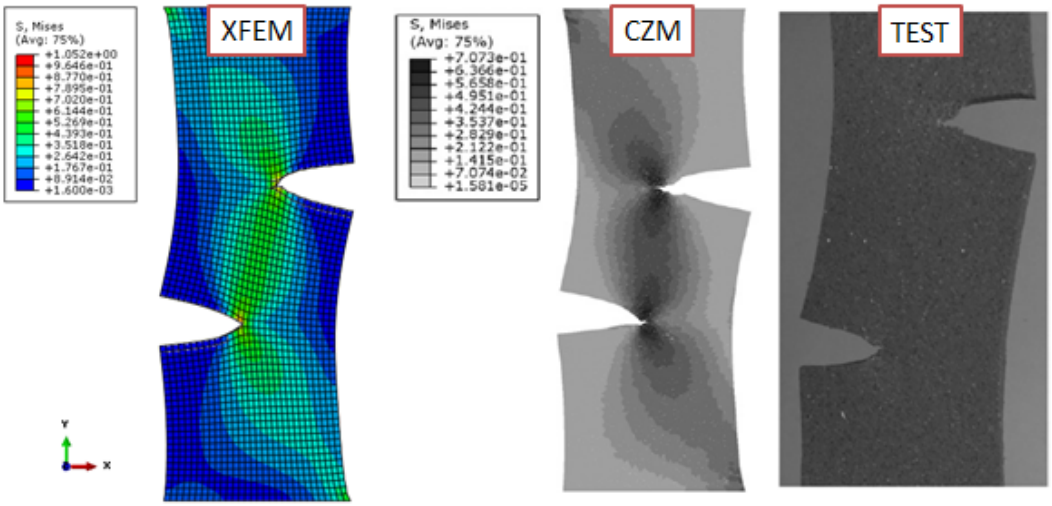

Figure 2.13. Comparison of von mises stress contours and deformation shapes of XFEM and the results taken from the literature [4].

Figure 2.14 shows the comparison of reaction force histories for XFEM solution calculated in this study and CZM solution and test result taken from the literature [4]. XFEM solution stopped at time 34sec because of convergence problems.

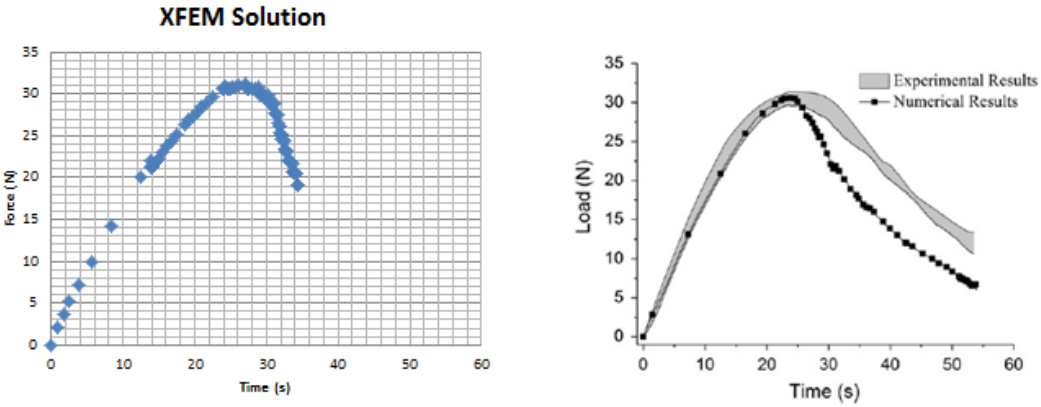

Figure 2.14. Reaction force vs. time: comparison of analysis results with the reference.

Based on the comparison with test results and CZM solution, it is verified that XFEM works successfully with linear viscoelastic material model.

2.4. Benchmark Study Conclusions

In this chapter, XFEM, CZM and conventional J integral methods were studied. Both traction - separation and LEFM damage models were employed. As a result of the comparison it is observed that the initiation and propagation times are similar for all of the methods. For traction - separation damage model, however, initiated crack faces are not fully separated, that is, the compression force between the crack faces is not zero. This is the likely case when the material is viscoelastic. Therefore, in this thesis study, as the material of interest is of nonlinear viscoelastic type, traction - separation damage model is selected to be more suitable than that of LEFM.

As was mentioned before, traction - separation model can be used with both CZM and XFEM depending on the problem. In this thesis study, we analyze two

different crack propagation problems in nonlinear viscoelastic media: bore crack and debonding. For bore crack, it is convenient to use XFEM since the crack trajectory is not known. For debonding case, however, CZM is appropriate since the crack is known to propagate along the interface between the case and the propellant.

3. BORE CRACK

3.1. Problem Description

In Chapter 2, different crack propagation analysis methodologies and crack zone damage models were studied. In Chapters 3 and 4, crack propagation analyses using XFEM and CZM will be applied to an analogue solid propellant motor whose geometry and material model are stated below. The geometry and material models will be used for both bore crack and debonding analyses.

3.2. Geometry

The analogue motor, SRM, has a cylindrical structure with a circular cross section [5]. It consists of a solid propellant, the grain, enclosed in a composite case. The cross sectional dimensions are shown in Figure 3.1.

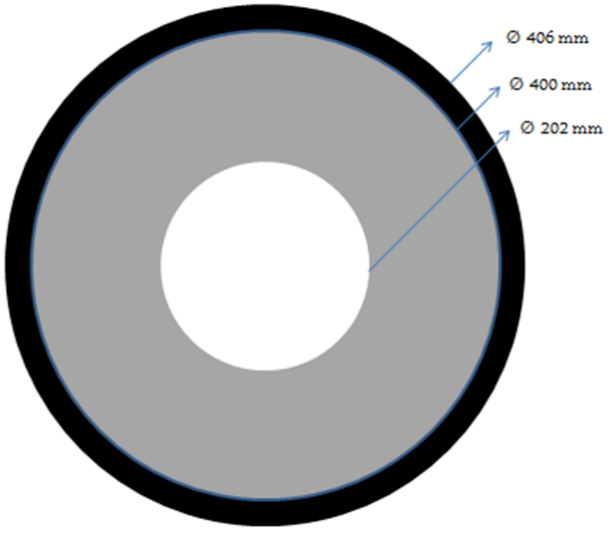

Figure 3.1. Analogue motor geometry for crack propagaiton analysis (ϕ: diameter).

3.3. Material Models

The SRM consists of two different materials. The grain is a nonlinear viscoelastic material and the case is a FRP (fiber reinforced plastic) material. The case is modeled as a linear elastic material with Young's modulus, E, Poisson's ratio, ν, thermal expansion coefficient, α, and stress-free temperature, Θ_0 whose values are given in Table 3.1.

Table 3.1. FRP case material properties [7].

E (MPa)	ν	α **(mm/C)**	Θ_0 $(^\circ C)$
4615.3	0.33	2.30E-6	20

The constitutive model for the propellant was taken from the literature [7] and is prosented in detail in Section 3.3.1.

3.3.1. Nonlinear Viscoelastic Material Properties

Realistic representation of the mechanical behavior of solid propellants requires nonlinear viscoelastic constitutive theories. The nonlinear viscoelastic model used in this study combines viscoelasticity with a hyperelastic model. The hypereleasticity is defined using strain energy function U in Yeoh form [36].

$$U = \left[3.7694 \times 10^{-1}(I_1 - 3) + 1.3243 \times 10^{-1}(I_1 - 3)^2 - 1.8037 \times 10^{-1}(I_1 - 3)^3\right] + \left[\frac{1100}{2}(J^{el} - 1)^2\right] \frac{kg}{mm^2} \tag{3.1}$$

where I_1 is the first deviatoric strain invariant and J^{el} is the elastic volume ratio. The coefficients of U are found by fitting the constitutive model to a uniaxial constant strain rate test data with superimposed pressure corresponding to the highest pressure the propellant is exposed to. This test is assumed to represent the material response without damage.

The viscoelastic material property is defined by a relaxation function expressed as a Prony series in the dimensionless form

$$g_R(t) = 1 - \sum_{i=1}^{N} g_i^P (1 - e^{-t/\tau_i^G})$$

where g_i^P and τ_i^G are material constants given in Table 3.2.

Table 3.2. Normalized Prony series for NLVE material [7].

N	g_i^P	τ_i^G **(min)**
1	0.3168635	1.00E-06
2	0.36025936	1.00E-05
3	0.16311863	1.00E-04
4	0.07820935	1.00E-03
5	0.02805517	1.00E-02
6	0.01822964	1.00E-01
7	0.00957705	1
8	0.00535763	1.00E+01
9	0.00041825	1.00E+02
10	0 0.0019107	1.00E+03

The equilibrium and instantaneous shear moduli are $G_\infty = 1.17 \times 10^{-1} kg/mm^2$, $G_0 = 6.507 kg/mm^2$, respectively.

The dependence of viscoelastic properties on temperature is defined by a shift factor determined from several relaxation test data of the propellant. The shift function, a_T, is represented in Williams–Landel–Ferry form as [18]

$$log a_T = -\frac{10.60(\theta - 20)}{235.58 + (\theta - 20)} \tag{3.2}$$

The coefficient of thermal expansion for the propellant is $\alpha_{pro} = 0.87 \times 10^{-4} 1/°C$ and the reference is $\theta_0 = 20°C$.

3.3.2. Damage Model for Crack

For the propagation analysis, traction - separation damage model was used. For the traction separation model two parameters are important: first one is the maximum stress value which determines the crack initiation, the other is the fracture energy which is the energy needed for complete separation of the new crack faces. Figure 3.2 shows the traction – separation behavior of the propellant material of interest. The fracture energy value was taken from [4]. The critical traction value is determined so that the crack growth can be observed clearly during the crack propagation analyses for several initial crack sizes. t_c and G^c stand for critical traction and critical fracture energy respectively.

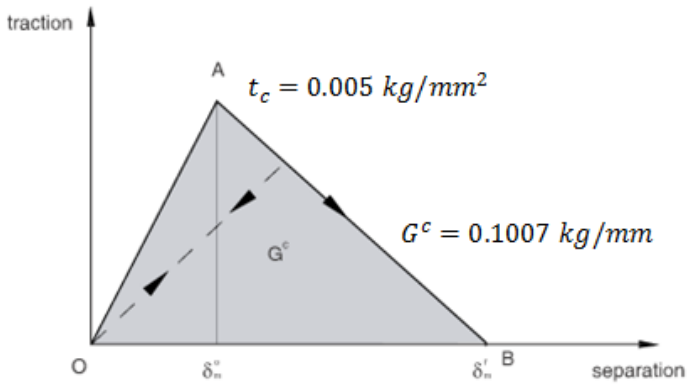

Figure 3.2. Traction - Separation curve of the propellant [4].

3.4. Effects of Bore Crack on Stress Distribution

In this section the effects of bore cracks on stress distribution over the cross-section were investigated for several crack sizes. Thermal loading was considered as described in Section 3.4.1.1. The results of the analysis were compared with the results from the literature [5]. The comparison was carried out qualitatively since the material

model of the referenced article is not known and probably different from the one used in our study.

3.4.1. Finite Element Model

In order to see the change in the bond stress along the 180 degree bond line, half of the cross section was used for the analysis. The analysis model consists of 13311 linear quadrilateral plane strain elements (CPE4). The FE mesh is shown in Figure 3.3.

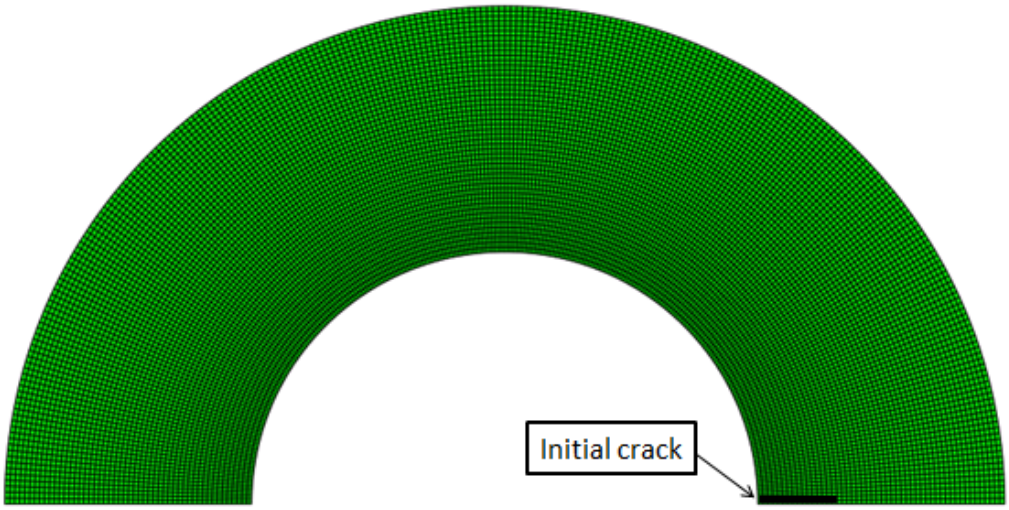

Figure 3.3. Finite element mesh for the bore crack analysis.

3.4.1.1. Boundary Conditions and Loading. Both ends of the half model are constrained in hoop (circumferential) direction of cylindrical coordinate system which is located at the center of the model. The loading is prescribed as decrease from $60°C$ to $20°C$ with a rate of 20 C/h.

3.4.1.2. Mesh Convergence. In order to determine a proper mesh size for the analyses, mesh convergence study was performed on the bore crack model (Figure 3.3). For the convergence study, 16mm, 8mm, 4mm and 2mm element sizes were employed using the

boundary conditions described above.

Figure 3.4 shows a convergence study result as a function of element size, h. The horizontal axis of the graph, 1/h, is proportional to the total element number. According to Figure 3.4, 4mm element size is determined as the converged mesh. For XFEM analysis, however, the smaller the element size is, the more sensitive the crack propagation calculation is. Therefore 2mm element size was used for all the analyses given in Sectin 3.4.2. The final mesh consists of 13311 bilinear quadrilateral plane strain elements (CPE4) and is shown in Figure 3.3.

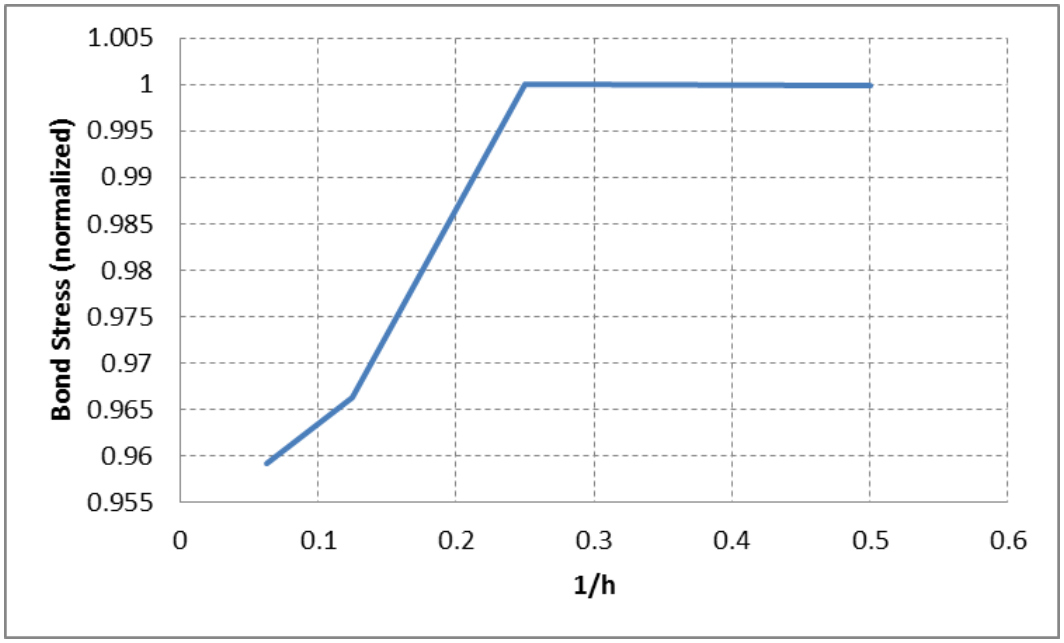

Figure 3.4. Mesh convergence plot.

3.4.2. Finite Element Analysis Results

Six different crack sizes were considered: 2mm, 4mm, 8mm, 16mm, 32mm, 64mm. For these cracks sizes, first, bond stress change along the circumference was calculated, second, the dependence of the difference between the maximum and minimum bond stress values along the bond line on the crack size was established.

3.4.2.1. Radial Stress Change. For all of the crack lengths, the radial stress along the bond line was plotted as shown in Figure 3.6. It was observed that, as the crack size is increased, the stress drop along the bond line also increases and far from the crack location the stress converges to a base value. These behaviors of the stress change play an important role on sensor systems that is used to monitor the crack presence in motors. Figure 3.5a shows such a sensor system that aims to determine the location and size of the bore crack using the readings at bond line. Figure 3.5b shows the bond stress distribution as predicted from finite element analysis [5], assumed to have used linear elastic material model at $20°C$.

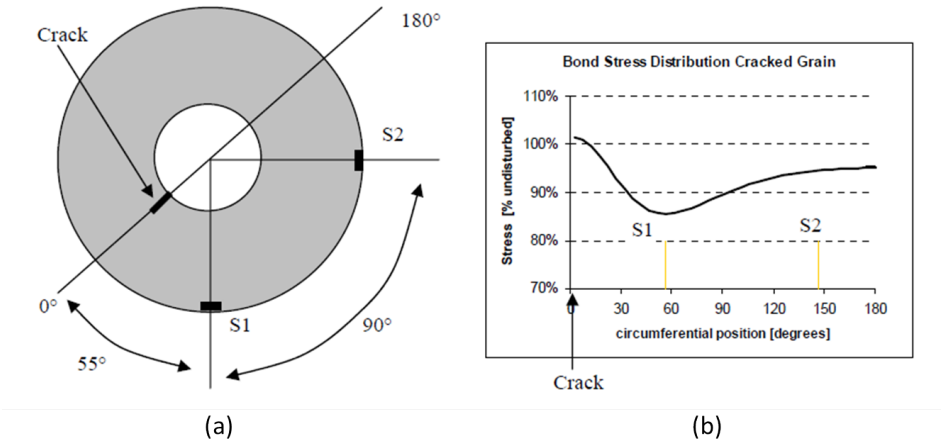

Figure 3.5. Location of sensors (a); Radial stress distribution along bond line for 5mm crack case (b) [5].

Comparing Figure 3.5b with Figure 3.6 qualitatively, it is observed that stress change along bond lines are similar. Since the dimensions of analogue motors of the referenced study and the current study are different, circumferential location of maximum drop is different and the maximum stress drop shown in Figure 3.5 (5mm crack case of referenced study) is almost identical to that in Figure 3.6 for 32mm crack. Figure 3.10 shows that, the stress curves of the materials of the current study and the referenced study are similar at $20°C$. Therefore the difference between current and the referenced study is due mainly to the differences in geometry of two analogue motors.

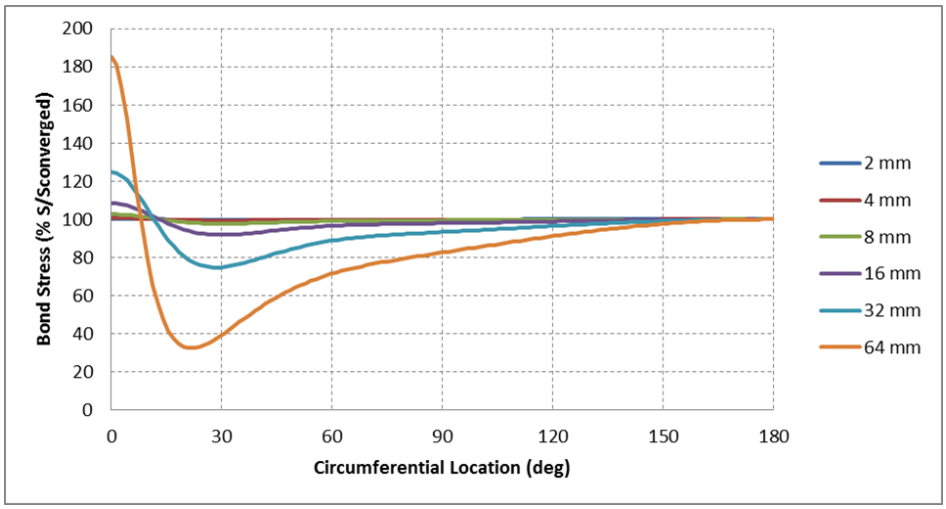

Figure 3.6. Radial stress distribution along bond line (current study).

The maximum stress drops along the bond line is given in Table 3.3 and plotted in Figure 3.7. It is concluded that the stress drop along the bond line is almost linearly proportional to crack length after 16 mm. Based on this curve, the crack size in the motor can be predicted using the sensor readings of any health monitoring systems.

Table 3.3. Maximum stress drop along bond-line for different bore crack sizes.

Crack Length (mm)	**Percent Stress Drop**
2	0.13
4	0.60
8	2.29
16	8.11
32	25.16
64	67.45

An example of stress distributions in radial and circumferential direction are shown in Figures 3.8 and 3.9 for 32mm crack case.

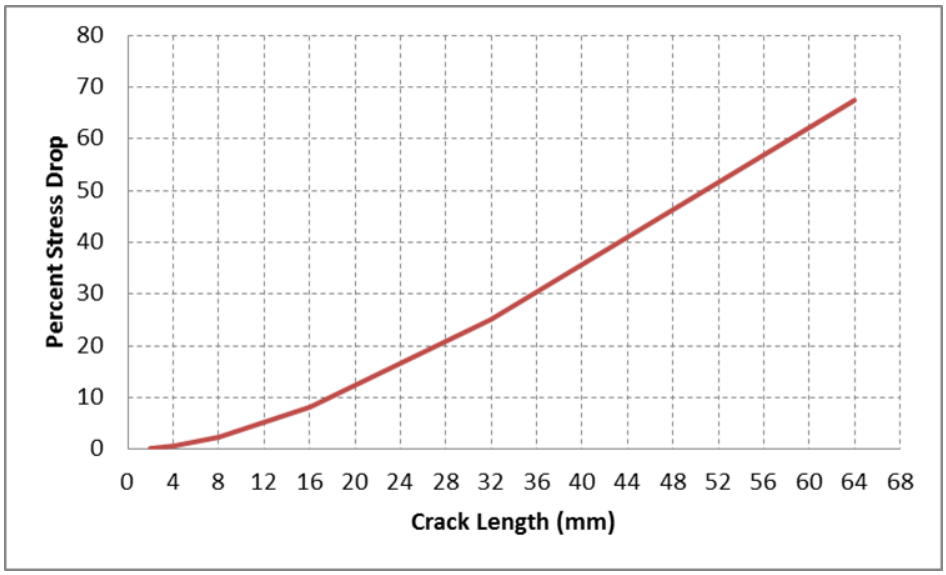

Figure 3.7. Crack length vs. bond stress.

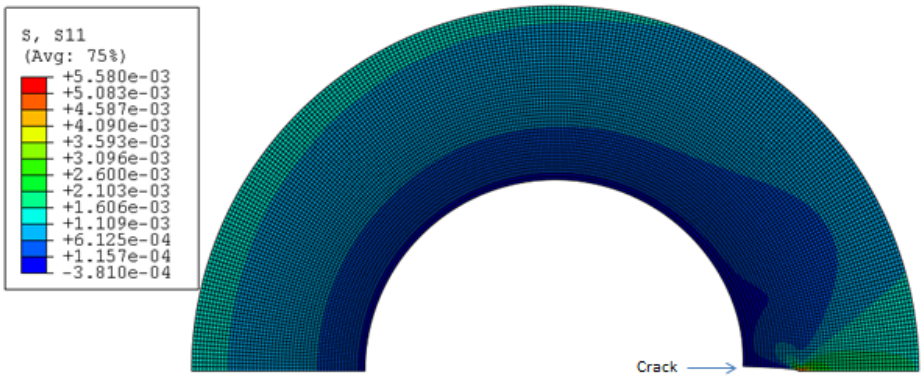

Figure 3.8. Contour plot of S11 for 32mm crack.

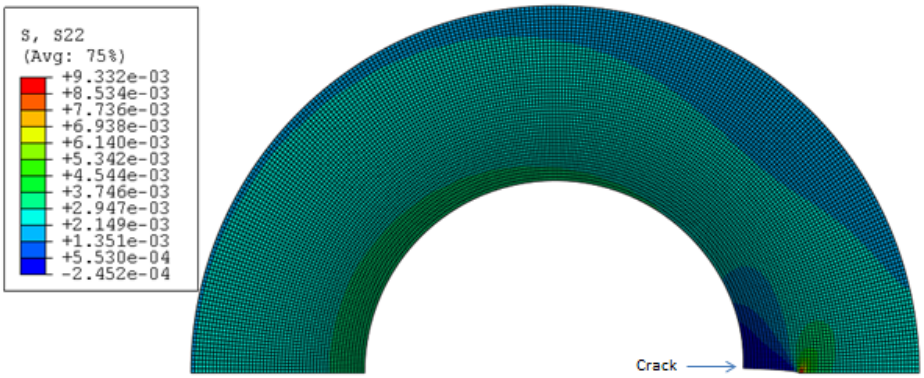

Figure 3.9. Contour plot of S22 for 32mm crack.

3.4.2.2. Uni-axial Tension Test. The uni-axial tension behavior of the propellant material was simulated. The load was applied at the strain rate of $0.7291 min^{-1}$ at several temperatures. Figure 3.10 shows the material responses predicted by the nonlinear viscoelastic material model used in the current study, test data from the referenced study and the LVE prediction of the referenced study [5]. Comparing the LVE response and the test data, it is clear that LVE prediction is poor after stain of 0.02. When the comparison is made between the test data and the NLVE material model of the current study, it can be concluded that the stiffnesses of the current material and the material of the referenced study are similar at $60°C$ and $20°C$. At $-40°C$, however, the current material is stiffer.

3.4.2.3. Cyclic Temperature Loading. The temperature loading shown in Figure 3.12 was applied to the motor and results were compared with those in the referenced study. The applied temperature profile represents the measured temperatures shown in Figure 3.11. The measurements from the sensors of the referenced study is shown in Figure 3.11. Radial stress calculated in the analysis is shown in Figure 3.13.

As a result of the comparison, it is concluded that the peak stress value is decreasing in the proceeding cycles as a result of the viscoelastic properties of the material.The stress drop is not as noticeable as the referenced document since the nonlinear viscoelastic model used in the current analysis does not account for the softening of

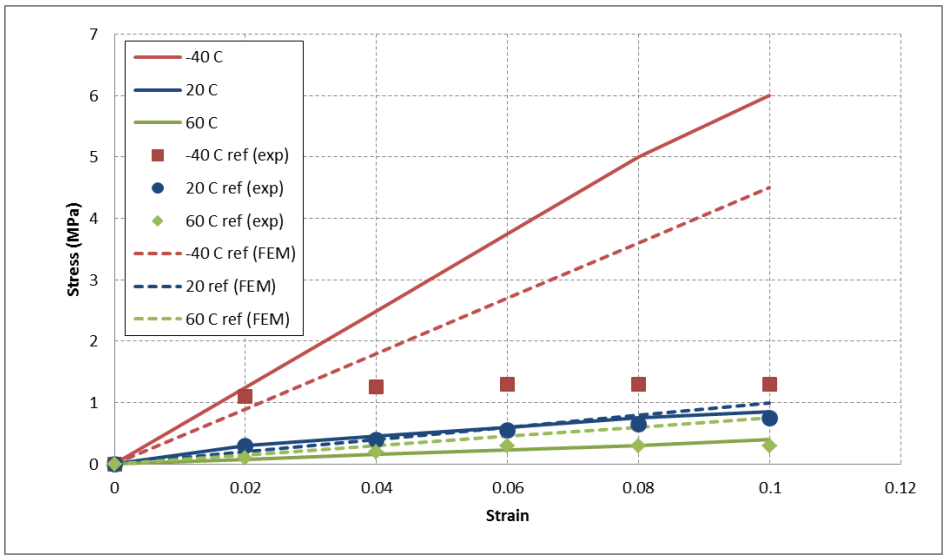

Figure 3.10. Material responses for uniaxial tension at constant strain rate of $0.7291 min^{-1}$ [5].

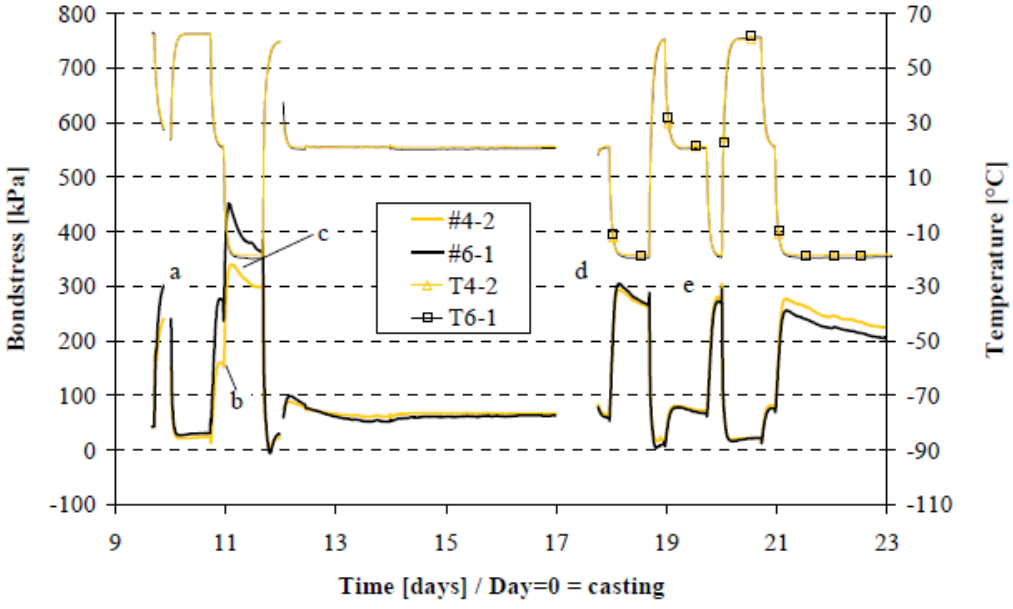

Figure 3.11. Measured temperature profile and the measured bond stresses during mechanical aging test of the motor [5].

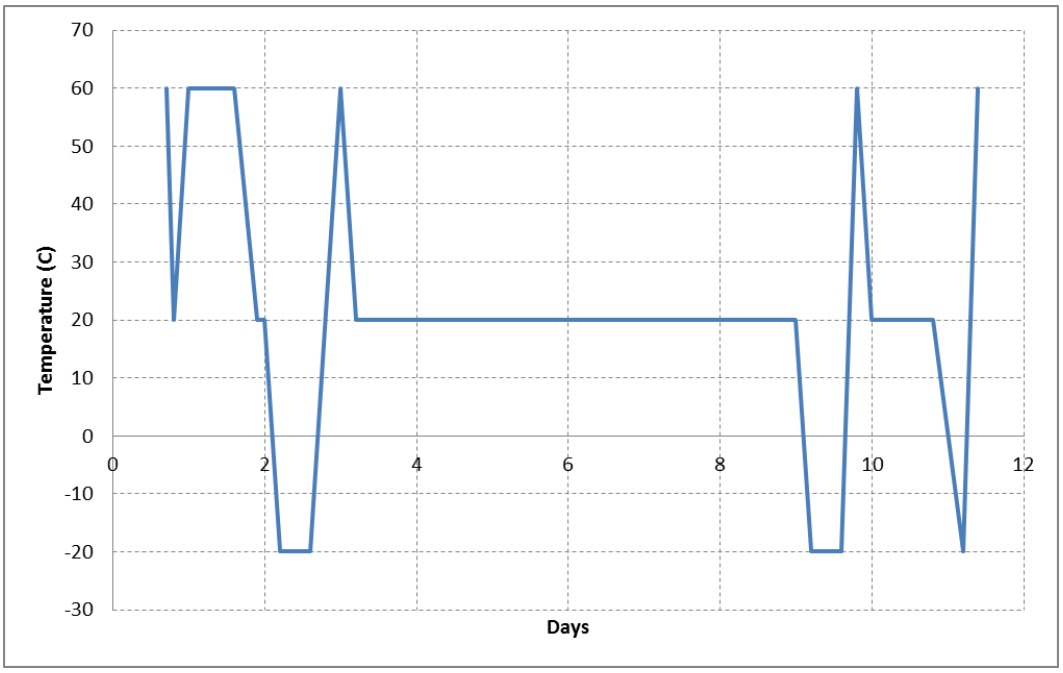

Figure 3.12. The temperature profile of the FEA.

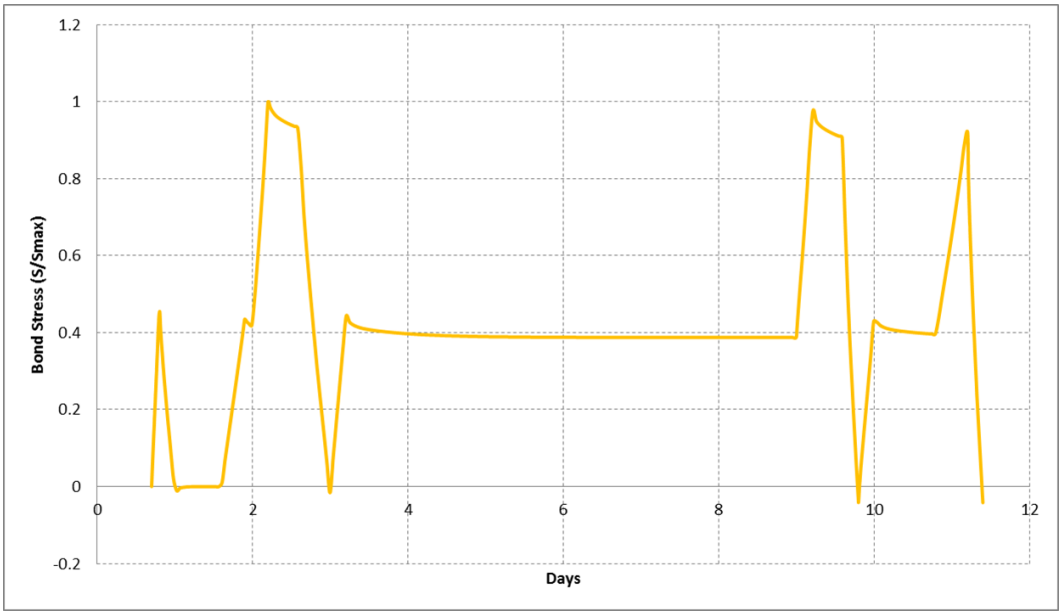

Figure 3.13. Bond stress history of the current study.

the propellant as seen in Figure 3.10. The decay in the peak stress values is shown in Table 3.4. Ratios in the table are relative to the stress value of the first cycle.

Table 3.4. Peak stresses corresponding to loading cycles in Figure 3.12.

Load (C)	**cycle**	**Ratio % (Test)**	**Ratio % (Analysis)**
20	a	100.0	100.0
20	b	72.0	98.8
-20	c	100.0	100.0
-20	d	87.0	97.7
-20	e	79.0	92.0

3.5. Bore Crack Propagation

The propagation of bore cracks in an analog motor as a result of cyclic temperature was analyzed using XFEM. Several initial crack sizes were examined. For each crack configuration, crack growth and stress distribution were calculated.

3.5.1. Finite Element Model

In the analysis, half of the circular cross section of analog motor is used. Since XFEM in ABAQUS does not support quadratic elements, 4-node plane strain full integration elements were used. The mesh consists of 13311 elements as shown in Figure 3.14.

3.5.1.1. Boundary Conditions and Loading. Since half of the cross section is modelled, at both ends symmetry boundary condition was applied in hoop direction of the cylindrical coordinate system whose origin is at the center of motor. The initial crack was located at 90° position.

The temperature profile is shown in Figure 3.15. The motor starts cooling from

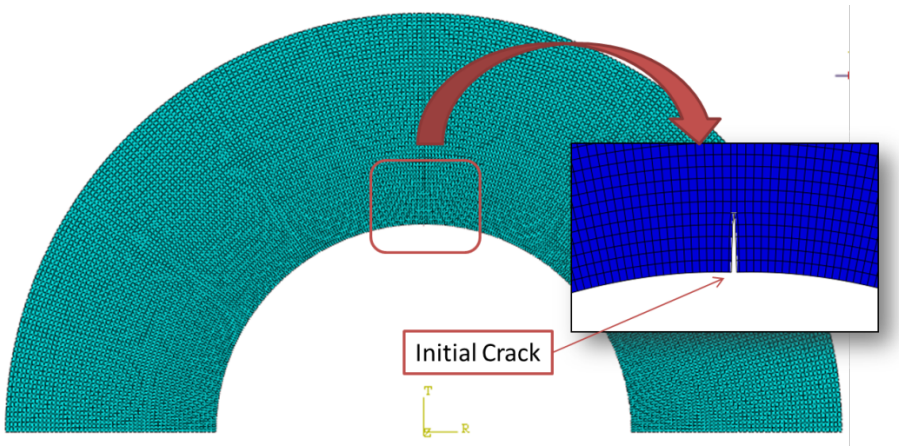

Figure 3.14. Analysis model.

60 C which is the stress free temperature. Then the temperature decreases to 20 C, 0 C, -20 C, -40 C and then increases in the reverse order with 2 hours of waiting between each temperature level and at the rate of 20 C/h. This cycle is repeated three times.

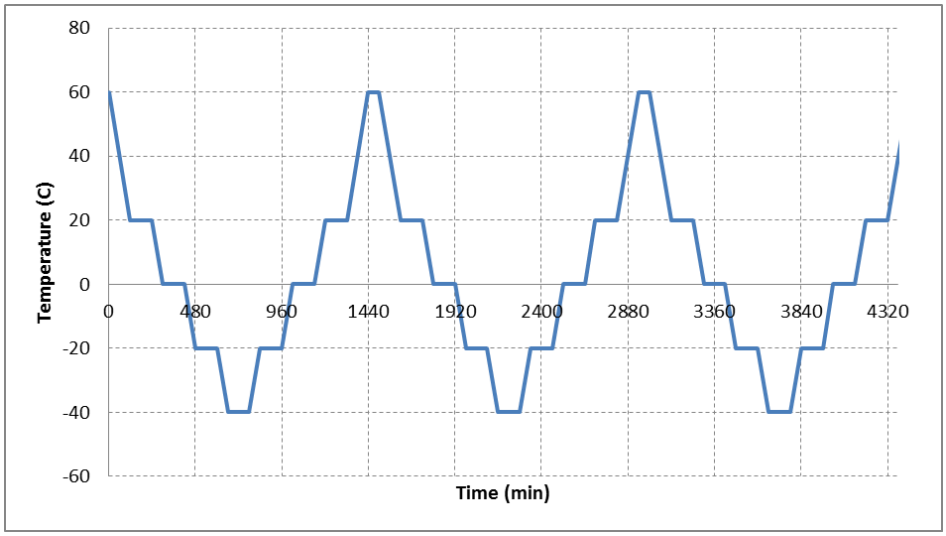

Figure 3.15. Cyclic temperature loading.

3.5.2. Using XFEM in Bore Crack Problem

3.5.2.1. Element Size. Crack propagation using XFEM occurs in somewhat discrete manner. That is, crack propagates throughout the element and it does not stop inside

an element. Therefore, the sensitivity of a growing crack is limited to the element size of the crack domain. For example, consider a crack of length 12 mm. If the element size is 2mm, then the crack increases as 12mm, 14mm, 16mm and so on. If the element size is 4mm, then the crack size would be 14mm, 16mm, 18mm and son on. In order to observe how the propagation history differs for different element sizes, 2mm and 4mm element were employed for a 12mm crack with the loading profile shown in Figure 3.16. The resulting propagation history is presented in Figure 3.17. It is observed that, although the curves are almost overlapping with each other, final status of the crack is different for the two cases. For 2mm mesh, propagation of the crack stopped at 26mm at the end of the load step while for 4 mm crack, the final crack size is 28mm. Because of this difference, 2mm mesh was used in this study.

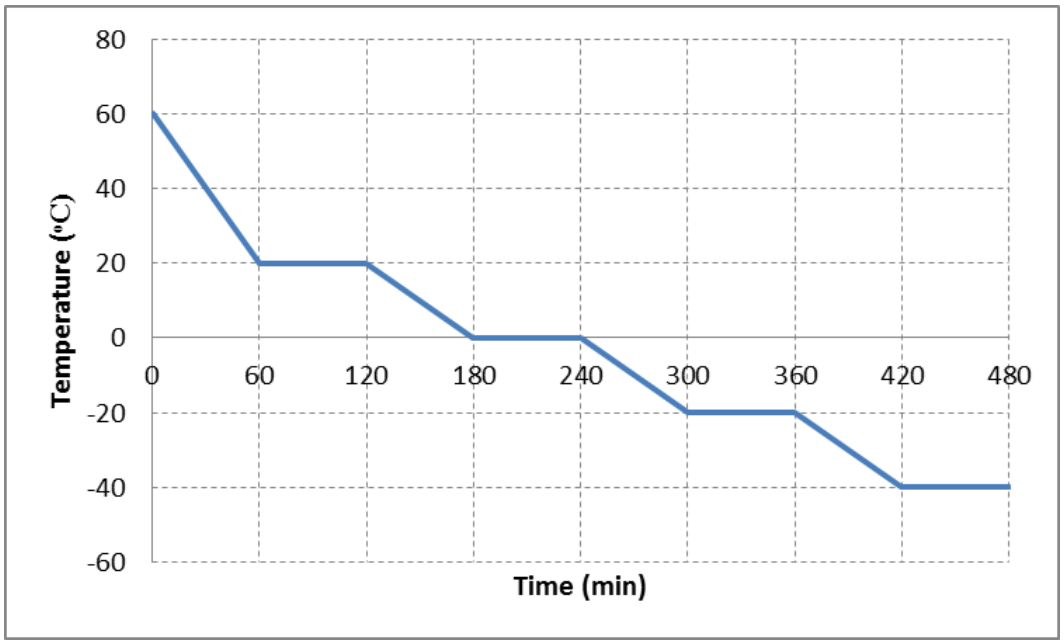

Figure 3.16. Loading profile for sensitivity analysis.

3.5.3. Finite Element Analysis Results

Six different crack sizes were analyzed under cyclic temperature loading shown in Figure 3.15. The initial crack lengths were 2mm, 4mm, 8mm, 12mm, 16mm and 32mm.

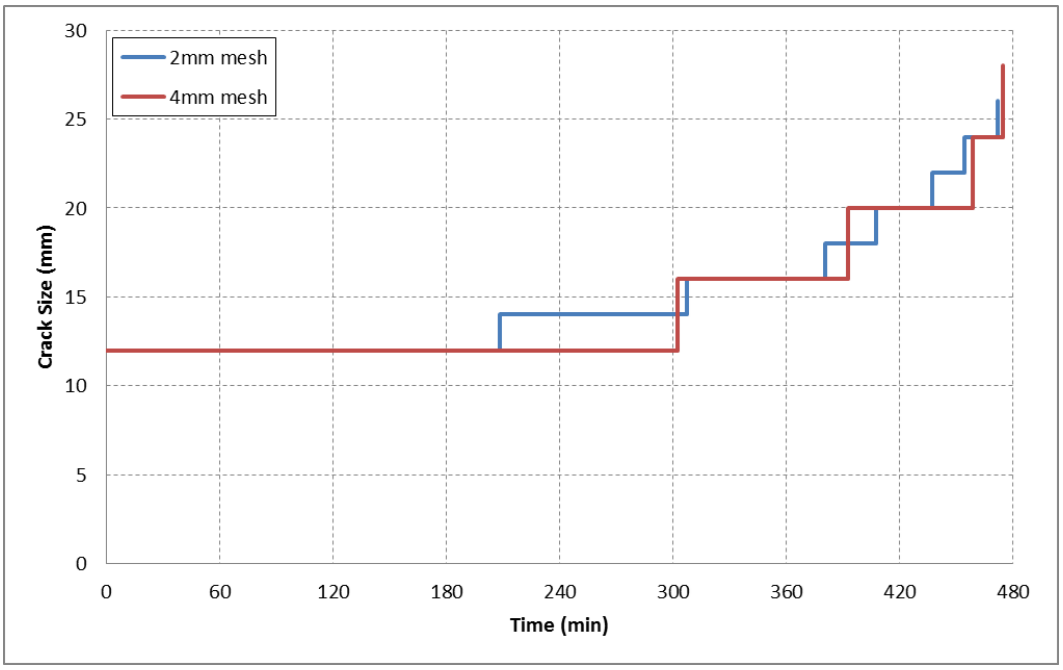

Figure 3.17. Crack propagation history for two different element sizes.

3.5.3.1. Cooling from 60 C to -40 C. The temperature profile consisted of cooling from 60 C to -40 C in the manner shown in Figure 3.15. The calculated crack propagation histories for different initial crack lengths are shown in Figure 3.18.

It is observed that crack is dependent on the initial crack size. That is up to some initial crack length (in this case 24 mm crack length), the crack growth increases with increasing initial crack length, after this point, crack growth decreases as shown in Figure 3.19.

Figure 3.20 shows the tangential stress distribution after crack growth. The blue regions in Figure 3.20 are the zero – stress regions which indicate the portions that reached to final separation (B point in Figure 3.2). The remaining portions of the cracks are still in the cohesive zone and require additional traction for full separation.

3.5.3.2. J Integral Solution for 4mm Initial Crack Size. The XFEM solution of the propagation analysis is compared with J integral approach. Figure 3.22 is energy

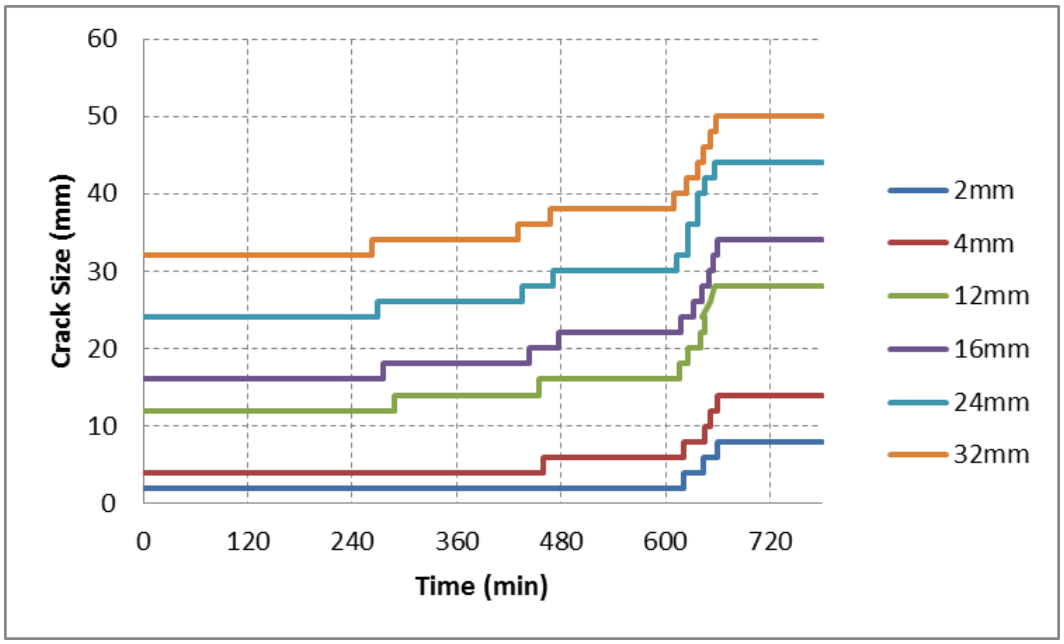

Figure 3.18. Crack propagation histories for various initial crack lengths.

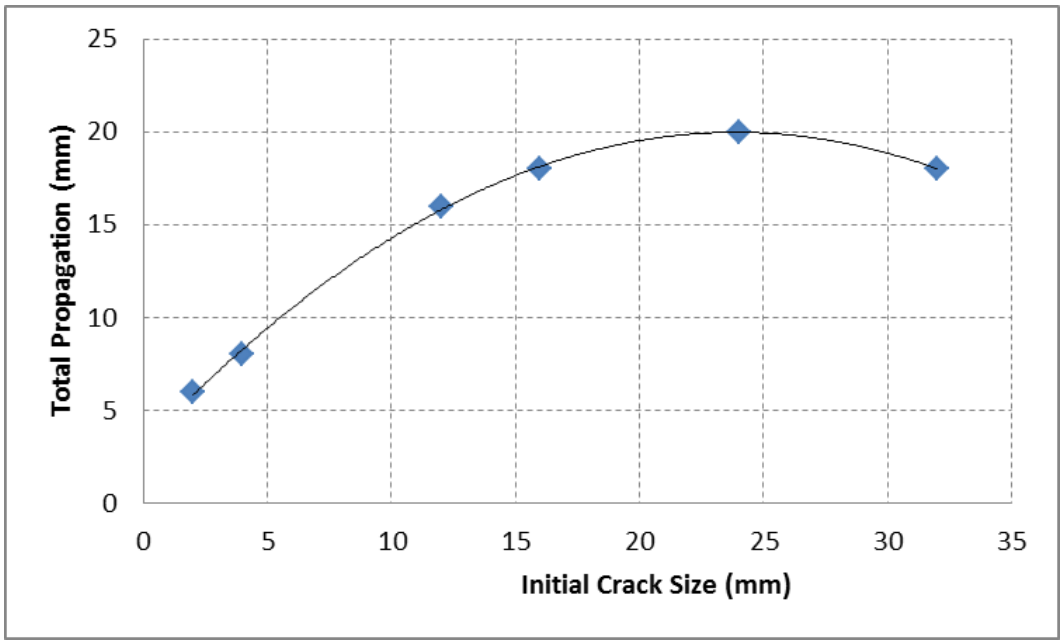

Figure 3.19. Increase in the crack size vs. initial crack size.

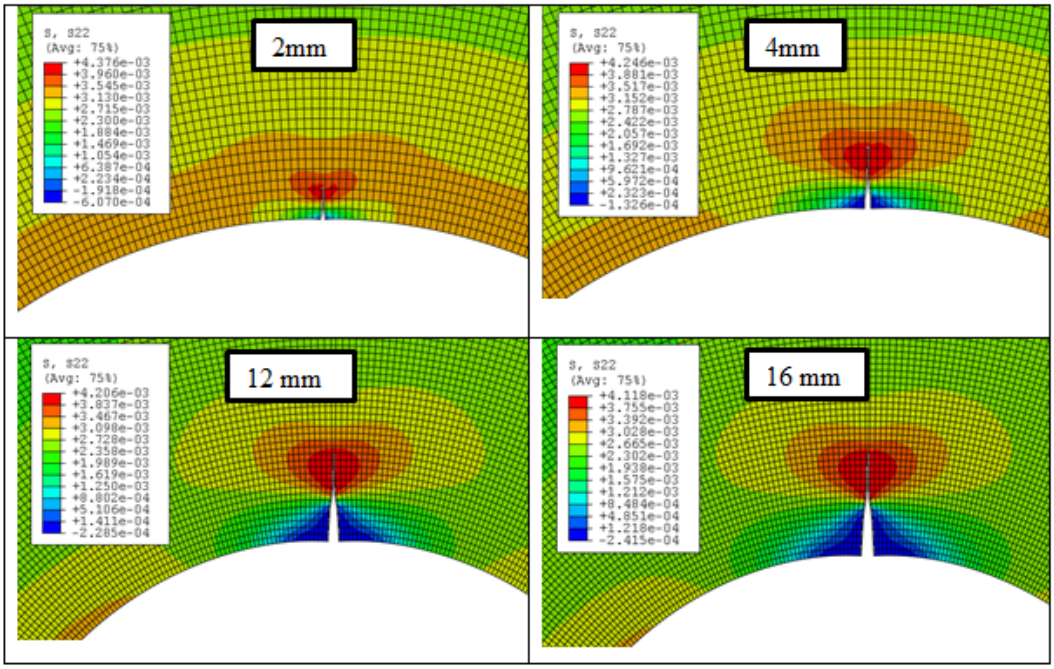

Figure 3.20. Circumferential stress distribution for various crack growth analyses (time t = 780 minutes).

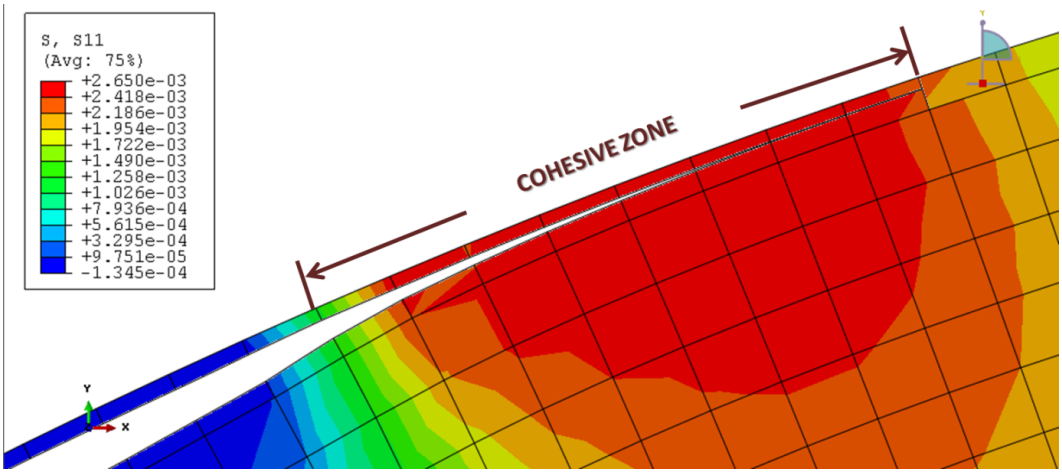

Figure 3.21. Representation of the cohesive zone.

dissipation plot of XFEM solution of 4mm initial crack size case. The first propagation from 4mm initial crack size to 6mm occurs at 458th minute. The dissipated energy per unit area at that point is 0.45E-3 N/mm.

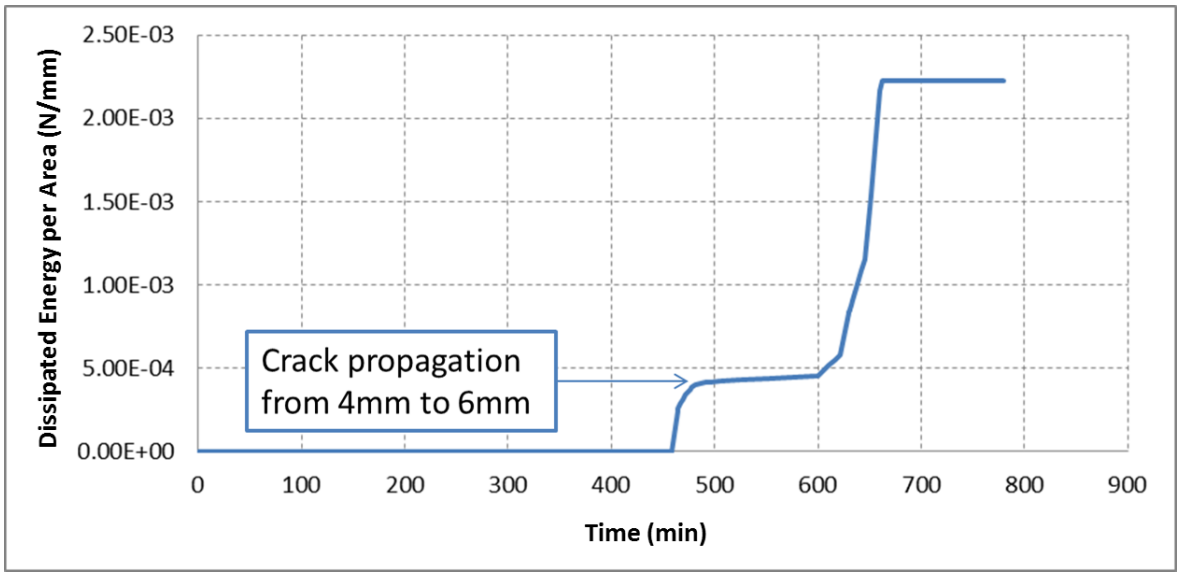

Figure 3.22. Energy dissipation resulting from XFEM solution.

Figure 3.23 is the change of J integrals of 4mm and 6mm crack sizes under the same loading conditions as the XFEM analysis upto the first propagation time (458th minute).

It is observed that, the XFEM solution is in good correlation with the J integral approach. While the dissipated energy during the first propagation step of XFEM solution (from 4mm to 6mm) is 0.45E-3, the J integral difference at that time of stationary analysis is 0.47E-3 N/mm.

3.5.3.3. Cyclic Loading. For cyclic loading of the models it is observed that for all of the cases, crack propagation occurred only during the cooling part of the first cycle. Since neither damage accumulation was modeled nor fatigue calculation was included in the analysis, crack did not propagate in the proceeding cycles. Similarly the peak stress reached at each cycle remained the same. This can be seen in Figure 3.24 which

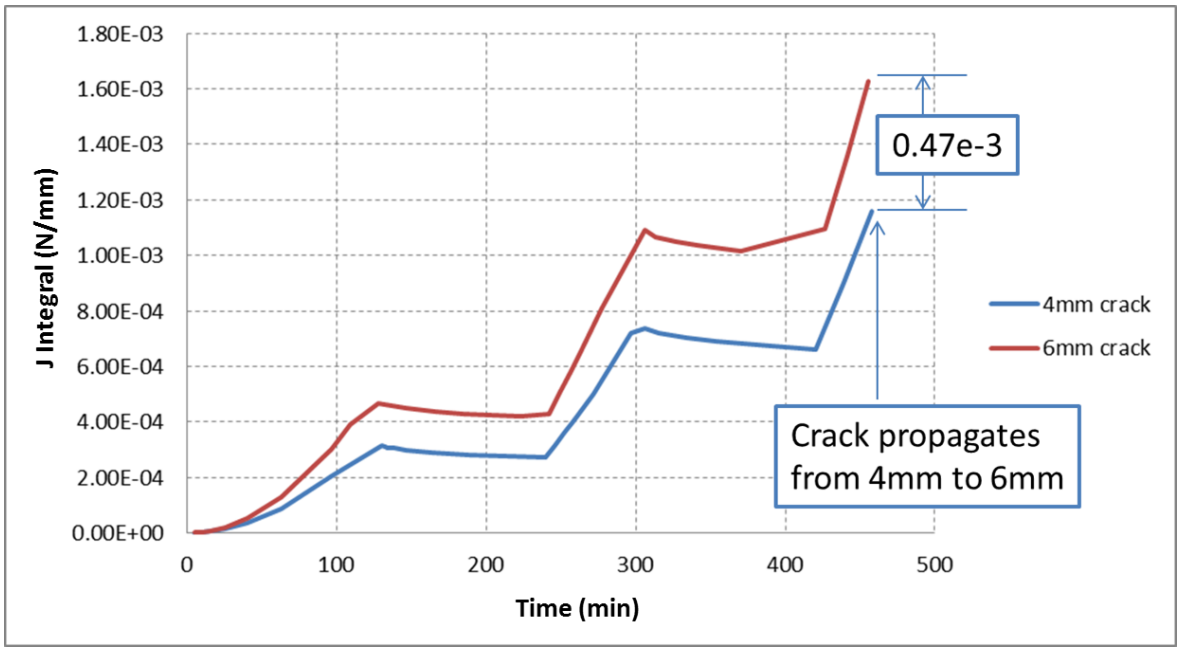

Figure 3.23. J integrals for 4mm and 6mm stationary crack analysis.

shows the circumferential stress history at the crack tip for cyclic loading and 4mm initial crack length.

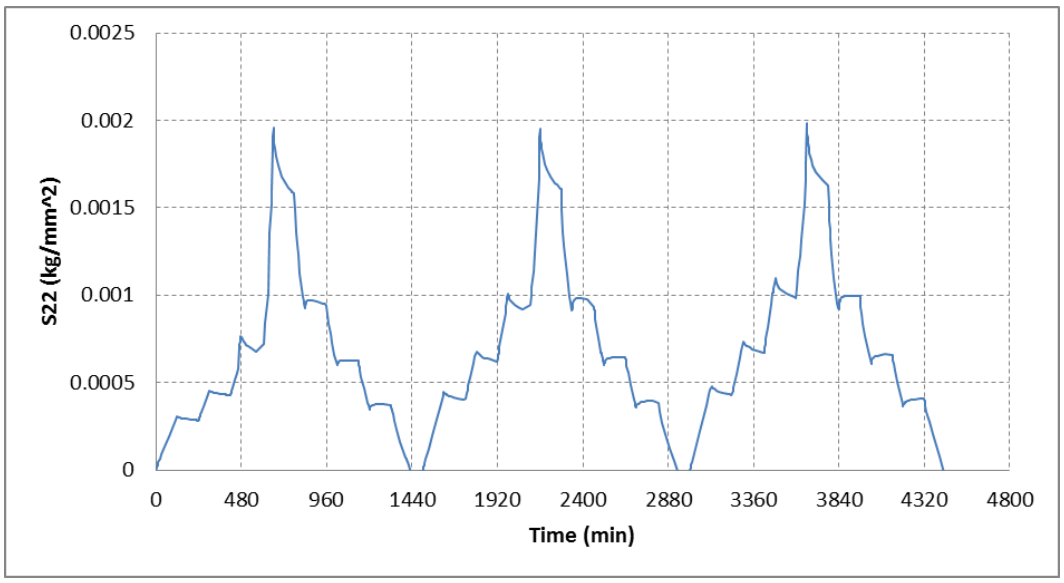

Figure 3.24. Circumferential stress change at the crack tip during the cyclic loading (4mm initial crack case).

4. DEBONDING

4.1. Effects of Debonding on Bond Stress Distribution

Debonding along the grain-case interface is one of the major failure modes of solid propellant rocket motors. As the temperature varies during cooling or heating, because the thermal expansion coefficients are different for the case and the propellant, thermal strain which these two materials experience will be different. This difference causes tension in radial direction at the bond line. When this stress exceeds the strength of the insulation material or propellant material, crack initiation (namely debonding) will take place which, in turn, will alter stress distribution along the bond line. The profile of this stress change along the bond line is important for detection of these defects. An important objective would be [6] to establish a relationship between the radial stresses and the debonding. This relationship is used to decide if debonding is present in the motor depending on the sensor readings.

In this part of the study, using an analogue motor geometry crack propagation analyses were performed for 5°, 10°, 15°, 20° initial debonding angles. The geometry, applied temperature profile and initial debonding angles were taken from the literature [6]. In the referenced study, the analysis was performed using linear elastic material model as the propellant material. The analysis was repeated for the material of the current study using linear elastic, nonlinear elastic and nonlinear viscoelastic material models. Firstly, linear elastic solution of our material was compared with the linear elastic solution of the referenced study. Then, linear elastic and non-linear elastic material models are employed to model the propellant, stress analyses were performed and the results were compared. Finally, using the same model, the time and temperature dependent viscoelastic and hyperelastic material model (non-linear viscoelastic) is employed to see the effect of non-linear viscoelastic behavior of the propellant.

4.1.1. Finite Element Model

The analogue motor geometry is shown in Figure 4.1. Because of the symmetry, a quarter - model is used. The mesh is shown in Figure 4.2 and consists of 6528 bilinear quadrilateral plain strain elements with 2mm element.

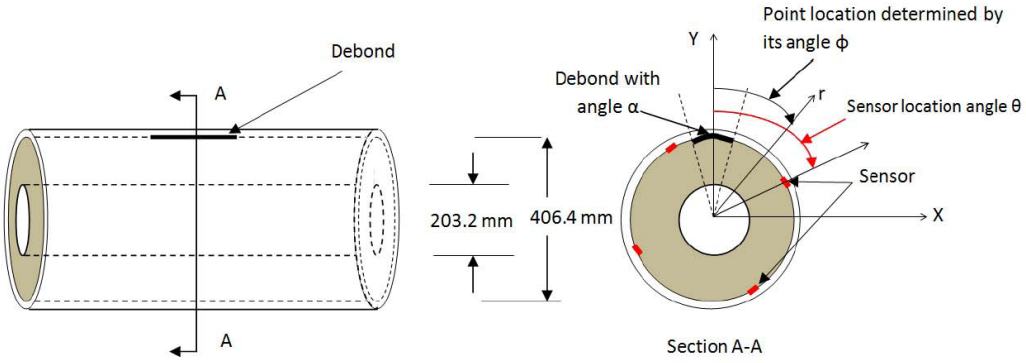

Figure 4.1. The analogue motor geometry [6].

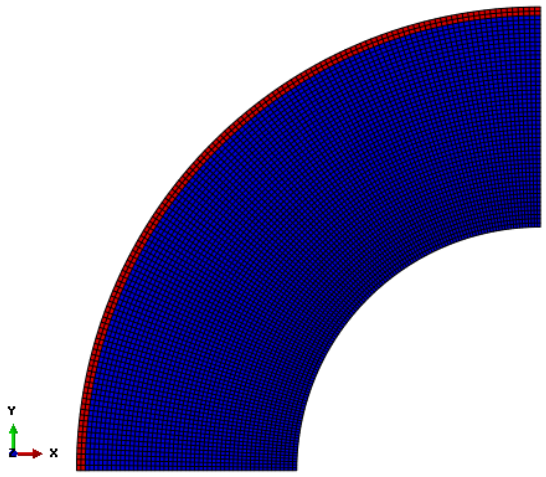

Figure 4.2. Finite Elements Mesh model.

4.1.1.1. Material Model. The SRM consists of two different materials. The grain is a nonlinear viscoelastic material and the case is a FRP (fiber reinforced plastic) material. The details for case material are given in Chapter 3, and material parameters are stated in Table 3.1. The propellant was represented with a linear elastic, nonlinear

elastic and nonlinear viscoelastic models, in order to see the effect of nonlinearity and viscoelasticity. The nonlinear viscoelastic material parameters are stated in Section 3.3.1. For nonlinear elastic model the energy function given in Section 3.3.1 was scaled by the instantaneous modulus. Linear elastic model consisted of the instantenous modulus and Poisson's ratio 6.05 kg/mm^2 and 0.49, respectively.

Before comparison of different material models firstly a uniaxial tension analysis is performed to compare stress-strain behaviours of the material models. In order for the comparisons made in Sections 4.1.2.1 and 4.1.2.2 to be meaningful, we expect that the linear portions of stress strain curves of the material models are identical in the elastic region. The uniaxial tensile response of four different material models (Linear Elastic, Nonlinear Elastic, Linear Viscoelastic, Nonlinear Viscoelastic) at strain rate of $10^{-4}min^{-1}$ is shown in Figure 4.3. From Figure 4.3, it is seen that initial portions of the stress strain curves of four different material models are identical as expected.

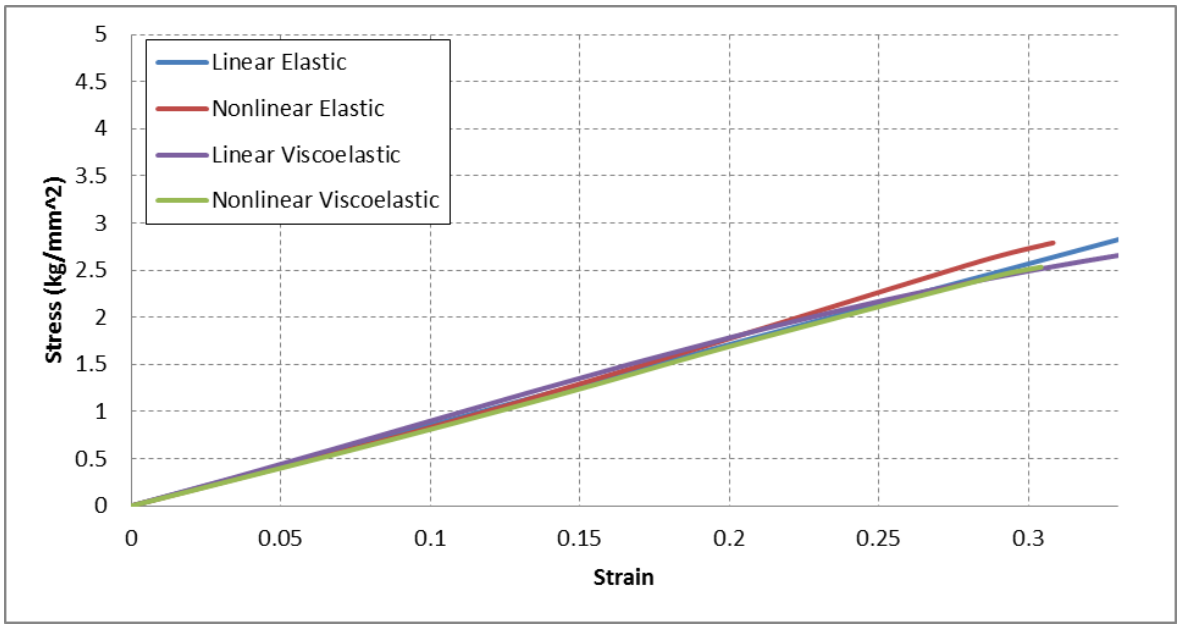

Figure 4.3. Stress - Strain curves as a result of uniaxial tension analyses for different material models.

4.1.1.2. Boundary Conditions and Loading. Because of the symmetry, a quarter - model is used. Both ends of the quarter model is applied symmetry boundary condition in circumferential direction. That is, both ends of the quarter model are constrained in circumferential direction. The problem is cooling of motor from 60 C to -40 C at the rate of 10 C/min. As mentioned above, as the rocket motor and the case undergo this cooling process, propellant shrinks more than the case which results in tension in radial direction along the bond line. The stress distribution of the propellant was calculated for four different debonding angles which are 5°, 10°, 15° and 20°.

4.1.2. Finite Element Analysis Results

Figure 4.4 shows the radial stress distribution for 20° debonding case of reference study and the current study. As shown in Figure 4.4, radial stress fields are qualitatively similar for both studies. The radial stress change along bond line for the reference study and the current study using linear elastic model is shown in Figure 4.5. According to Figure 4.5, it can be concluded that the stiffness of the current material is higher than that of the reference study since the stress values as a result of the same cooling history is higher for the current study. In Sections 4.1.2.1 and 4.1.2.2, the effect of nonlinearity and viscoelasticity are investigated comparing the bond-stress profile along the bond-line.

4.1.2.1. Effect of Nonlinearity in Bond-stress. Firstly linear elastic and non-linear elastic material models were used as the propellant material and bond-stresses were compared. Radial stress along the bond line for different debonding cases (5°, 10°, 15°, 20°), is plotted in Figure 4.6 for linear elastic and non-linear elastic material models and the stress values are shown in Table 4.1. Looking at the curves in Figure 4.6, it can be seen that for linear elastic material model, bond-stress experiences a drop from 15° to 30° far from the crack tip (tip point of debonding), then again increases and finally converges to a value which is the defect-free stress. Defect-free bond-stress of nonlinear elastic material is similar to that of linear elastic one. The percent stress drops with respect to the defect-free stresses is more meaningful for comparison purposes. The

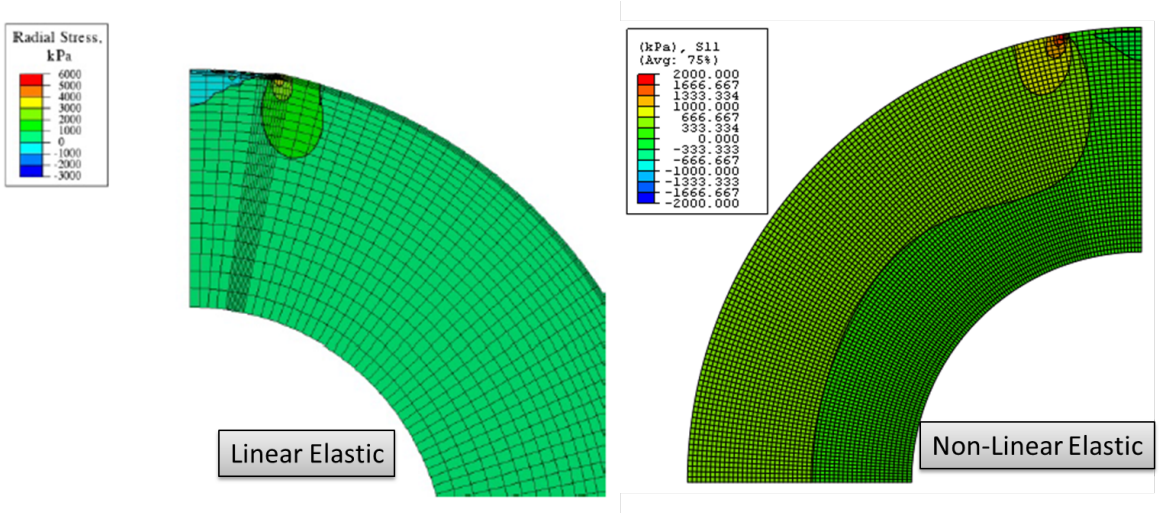

Figure 4.4. Radial Stress Distribution at -40 C of 20 deg debonding case of Referenced study [6] and the current study.

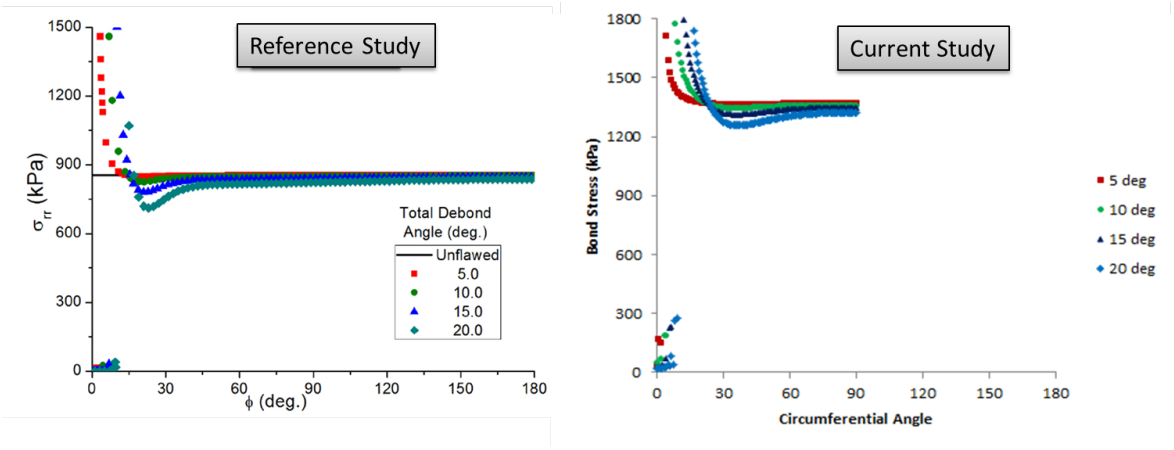

Figure 4.5. Stress change along the bond line for the linear elastic material model of the referenced study (left) and current study (right).

stress drop percentages given in Table 4.1 lead to the conclusion that slight difference is observed in predictions of linear and nonlinear models. From this result and the stress-strain curves in Figure 4.3, it can be concluded that the material response as a result of the applied temperature loading is in the linear region of Figure 4.3. The percentages of stress drops for different material models are compared in Figure 4.7.

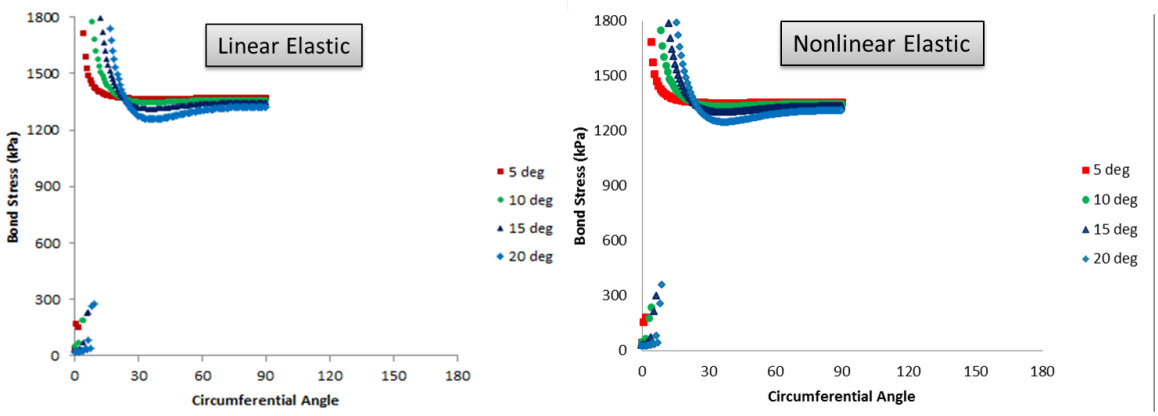

Figure 4.6. Radial stress changes along the bond for linear elastic and nonlinear elastic cases.

Table 4.1. Tabular representation of stress drops for the debonding cases (Linear elastic: Reference Study and Nonlinear elastic: Current Study).

	Linear Elastic		Nonlinear Elastic	
Unflawed Stress (kPa)	1350		1353	
	Min Stress (kPa)	% Drop	Min Stress (kPa)	% Drop
5 deg	1367	0.2	1350	0.2
10 deg	1348	0.6	1331	1.6
15 deg	1312	4.2	1296	4.2
20 deg	1257	8.2	1242	8.2

4.1.2.2. Effect of Viscoelasticity. Nonlinear elastic and nonlinear viscoelastic analysis results were compared. Figure 4.8 shows nonlinear elastic and nonlinear viscoelastic analysis results for cooling from 60°C to −40°C at 10°C/min cooling rate. The defect-

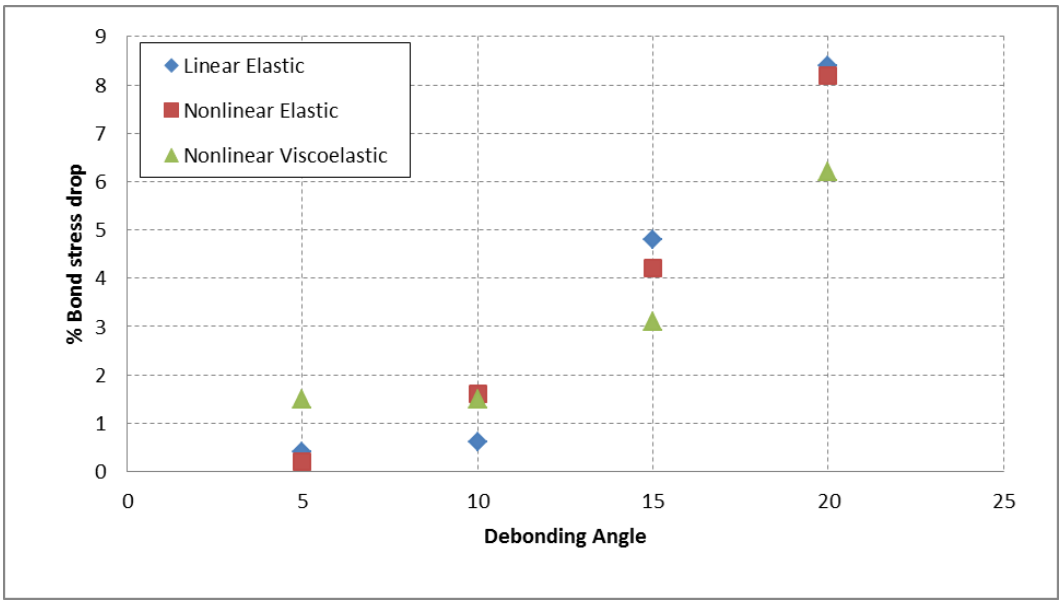

Figure 4.7. Percent stress drops for linear elastic, nonlinear elastic and nonlinear viscoelastic material types.

free radial stress decreases from 1350 kPa to 60 kPa when viscoelastic material model is used instead of elastic material model as the propellant material. This decrease in the bond-stresses is expected since the response of a viscoelastic material is rate dependent and thus changes as the cooling rate changes. Therefore, time dependent viscoelastic properties are necessary in order to properly model the rate dependence of non-linear viscoelastic propellant material. When bond-stress drops are compared as in Section 4.1.2.1 using the values given in Table 4.2, it is observed that percent stress drops are similar for the two material models as shown in Figure 4.7. Nevertheless, the nonlinear elastic material model, only approximately represent the propellant material and using nonlinear viscoelastic material model would be more suitable to represent material characteristics better.

4.2. Crack Propagation for Debonding

This section studies the debonding in solid rocket motors (SRMs) under cyclic temperature loading. The method used for the analysis is a CZM, in particular the surface based cohesive segment method which is based on bond contact of interface

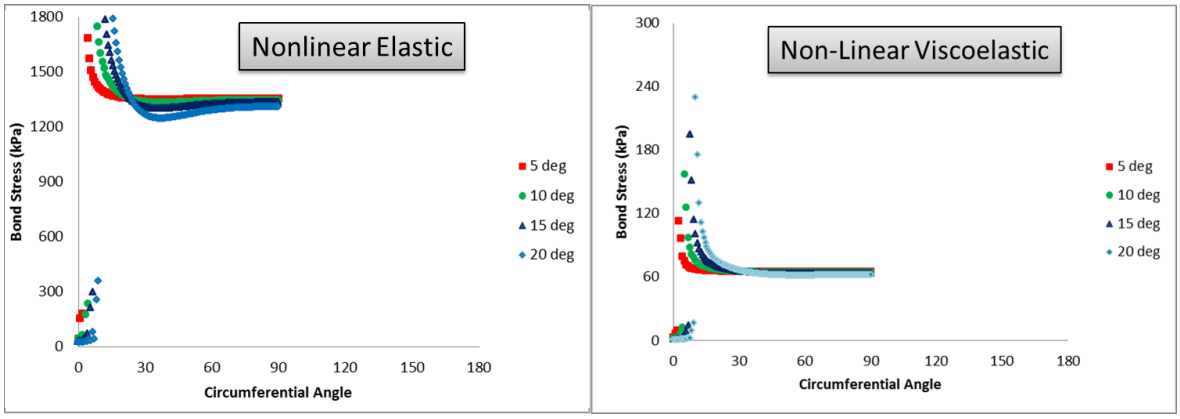

Figure 4.8. Radial stress changes along the bond for nonlinear elastic and nonlinear viscoelastic cases.

Table 4.2. Tabular representation of stress drops for the debonding cases (NonLinear elastic and Nonlinear Viscoelastic).

	NonLinear Elastic		NonLinear Viscoelastic	
Unflawed Stress (kPa)	1353		65	
	Min Stress (kPa)	% Drop	Min Stress (kPa)	% Drop
5 deg	1350	0.2	64	1.5
10 deg	1331	1.6	64	1.5
15 deg	1296	4.2	63	3.1
20 deg	1242	8.2	61	6.2

surfaces and the traction – separation damage rule. The details of this method is introduced in Chapter 3. For the analysis several initial debond angles were used to study the effect of initial debonding. For each of the cases the amount of the propagation versus analysis time was calculated.

4.2.1. Finite Element Model

For the analysis quarter slice of the entire cross section of the SRM is used as described in Section 4.1.1. The analysis model consists of 6528 bilinear quadrilateral plane strain elements (CPE4) as shown in Figure 4.9.

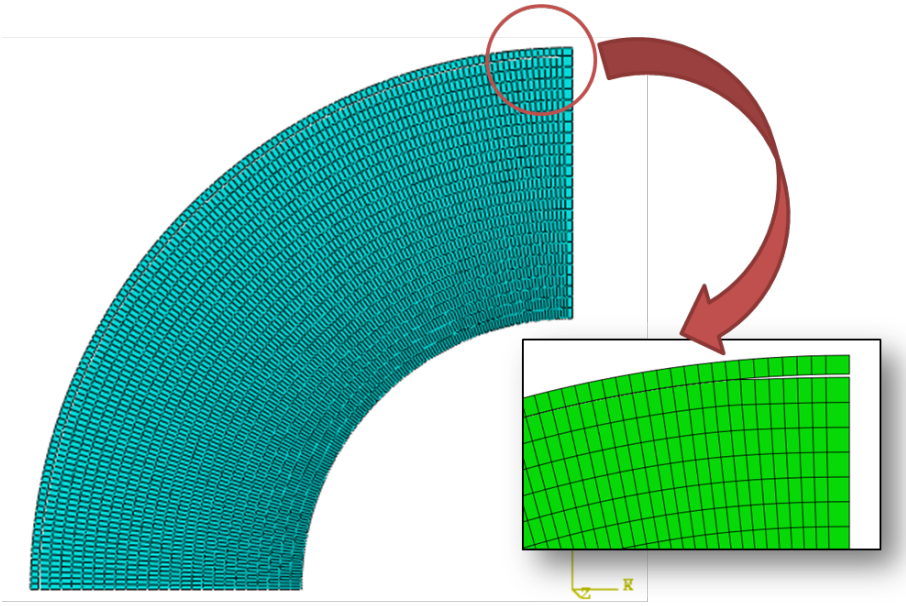

Figure 4.9. Analysis model.

4.2.1.1. Boundary Conditions and Loading. Since quarter of the cross section is used for the analysis, both ends of the quarter slice were applied symmetry boundary condition in hoop direction of the cylindrical coordinate system whose origin is at the center of motor. The initial crack was located at top-end of the quarter model as shown in Figure 4.9.

Applied temperature profile is shown in Figure 4.10. The stress free temperature is 60 C. That is, the model starts cooling from 60 C when there are no stresses throughout the model. Then the temperature drops to 20 °C, 0 °C, -20 °C, -40 °C respectively and heated up in the reverse order with at the rate of 20 °C/h with 2 hours of waiting between each temperature level. This cycle is repeated three times.

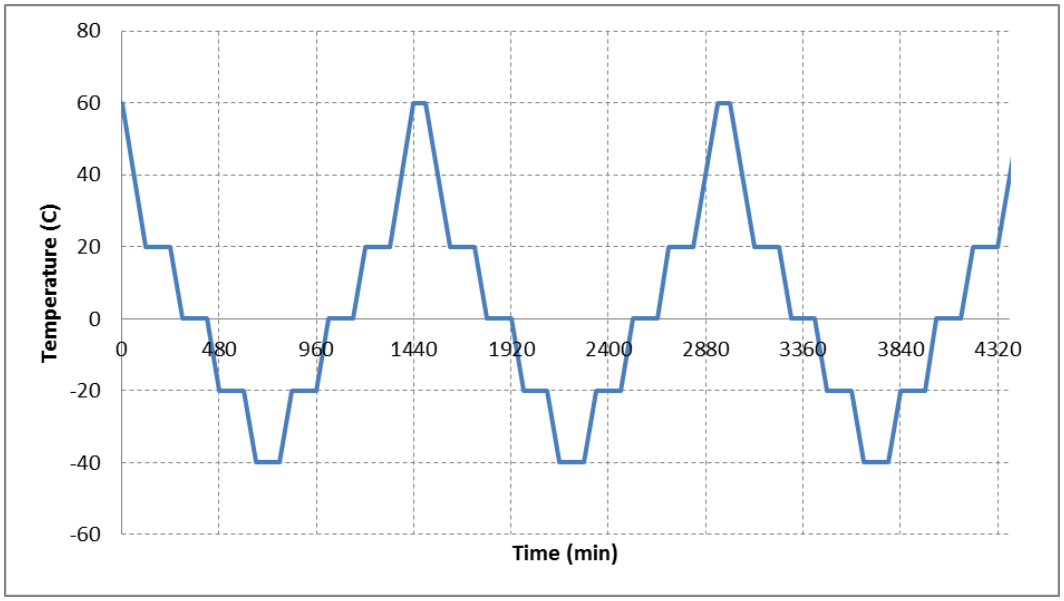

Figure 4.10. Analysis model.

4.2.2. Using CZM in Debonding Problem

The surface based cohesive segment method is based on the separation of the contact surfaces according to traction-separation damage model. The two bonded surfaces are initially in a contact at non-deboneded regions of the interface. As separation load is applied, the bonded surfaces are separated according to the damage model. That is, in this method, damage model is not a material property but the separation rule of the bonded contact. Since XFEM seems to pose difficulties when applied to the interface crack problems, CZM was chosen for the current problem.

4.2.2.1. Damage Model. Traction – Separation behavior of the material contains the information about the crack initiation and propagation conditions and the crack separation after the initiation. The traction - separation damage model was introduced in Chapter 2 and the traction separation curve is repeated in Figure 4.11.

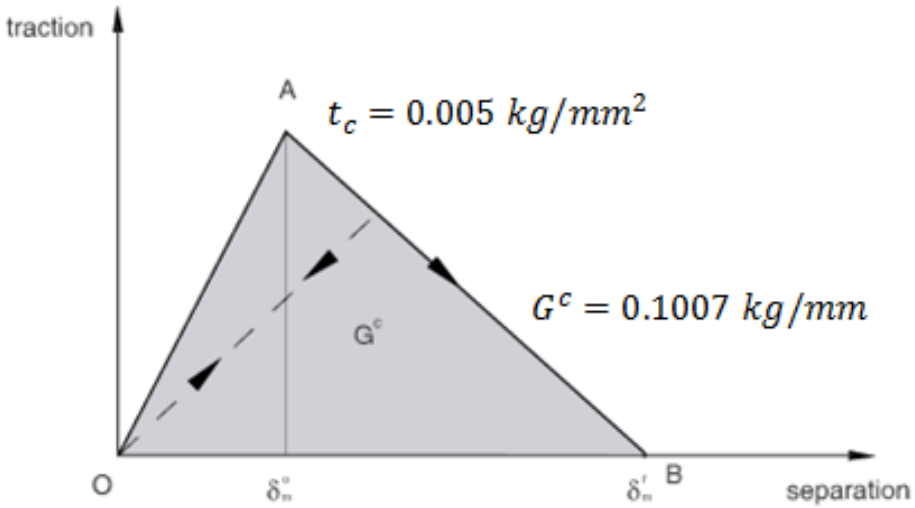

Figure 4.11. Traction - Separation curve of the propellant.

4.2.3. Finite Element Analysis Results

For the present study five different initial debond angles were studied. These are: 5°, 10°, 15°, 20° and 25°.

4.2.3.1. Cooling from 60 °C to -40 °C. Firstly only the cooling part (60 °C to -40 °C) of the temperature loading is applied to the model and crack propagation histories for different initial debonding angles are plotted as shown in Figure 4.12.

Surface based cohesive segment method allows easy post processing of the regions where the initiation occurs along the bond-line. The red regions in Figure 4.13 show elements where debonding has initiated.

Figure 4.14 shows the change of total propagation versus initial debonding angle.

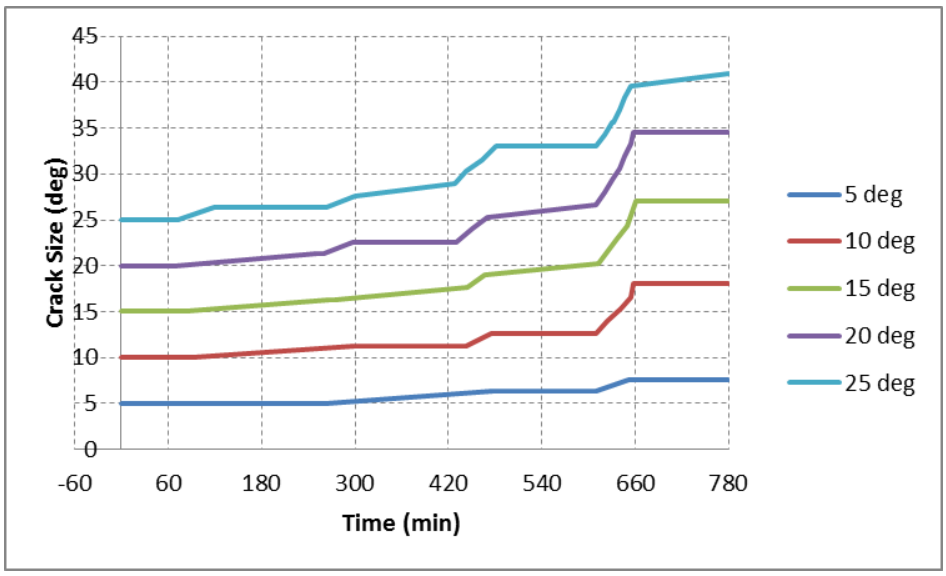

Figure 4.12. Crack size vs. Time plot.

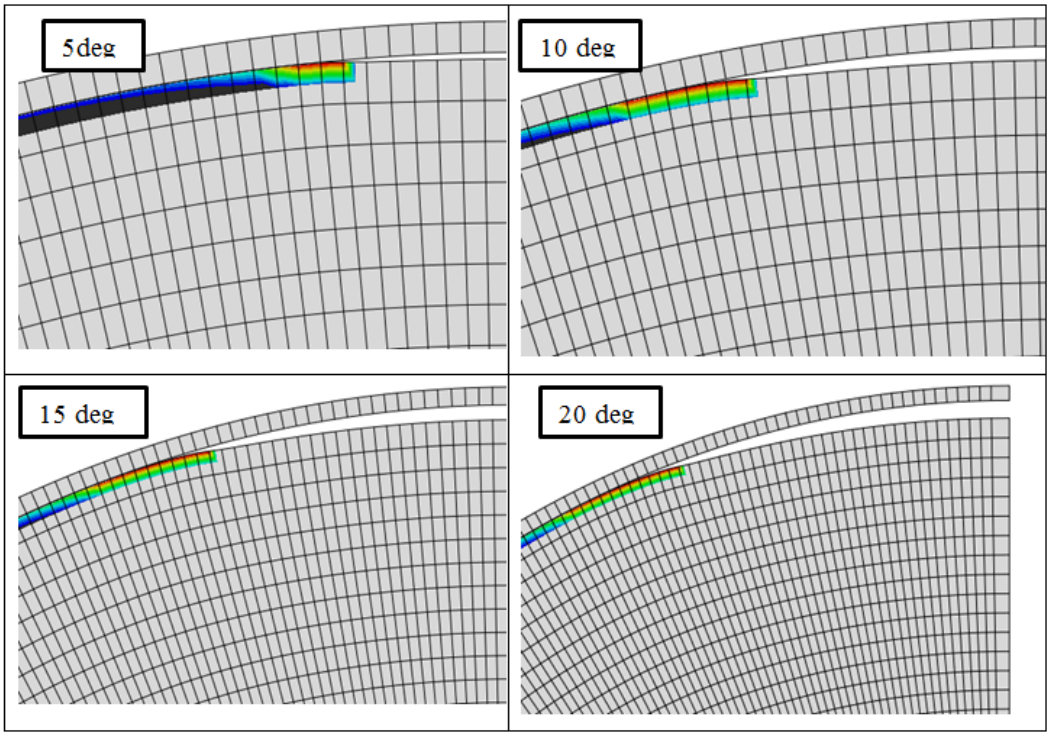

Figure 4.13. Enriched regions along the bond-line.

The dependence of the propagation size on the initial crack size shows parabolic behavior. As in the bore crack case, the propagation of debonding increases up to some initial debonding angle.

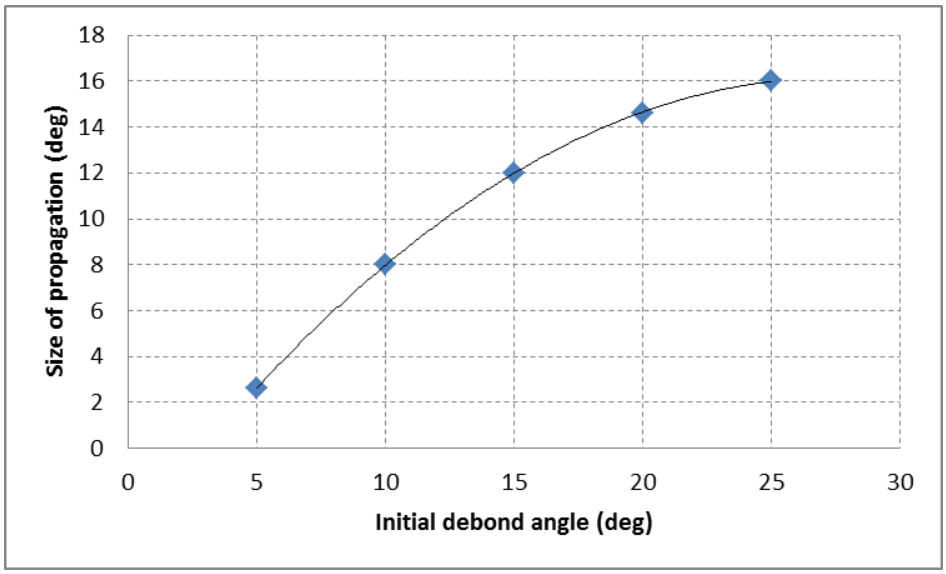

Figure 4.14. Increase in the crack size vs. initial crack size.

In Figure 4.15, the final state of the crack propagation and the radial (S11 of cylindrical coordinate system) stress distribution are shown. The blue regions are the zero – stress regions which indicate the portions of the cracks that reached to final separation (B point in Figure 4.11). The other portions of the cracks are still in cohesive zone and need additional energy for full separation as shown in Figure 4.16.

4.2.3.2. Cyclic Loading. For temperature cyclic loading it is observed that for all of the analysis cases, crack propagation occurred only during the cooling part of the first cycle. As an example, Figure 4.17 shows the radial bond stress history during the cyclic loading of 15° initial debonding case.

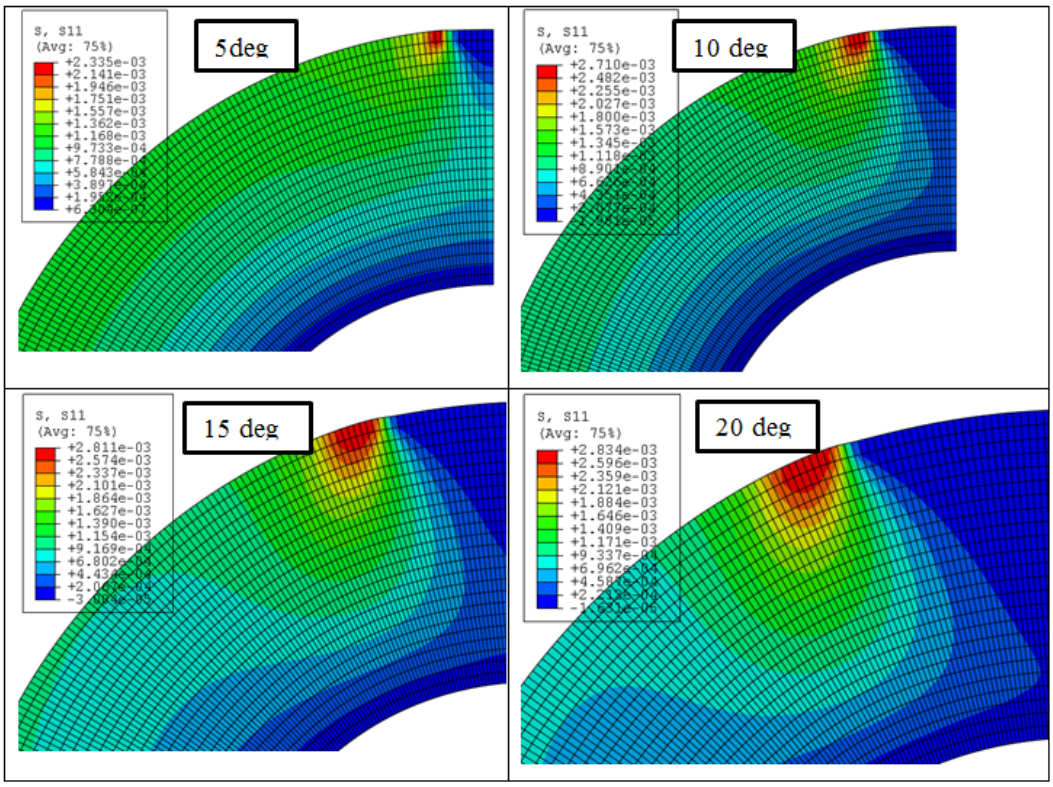

Figure 4.15. Final states of the propagation.

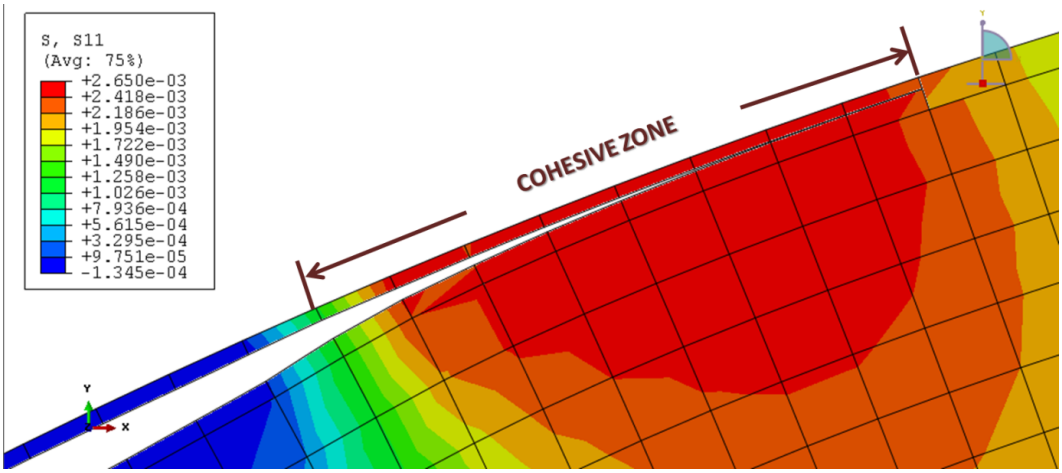

Figure 4.16. Representation of the cohesive zone.

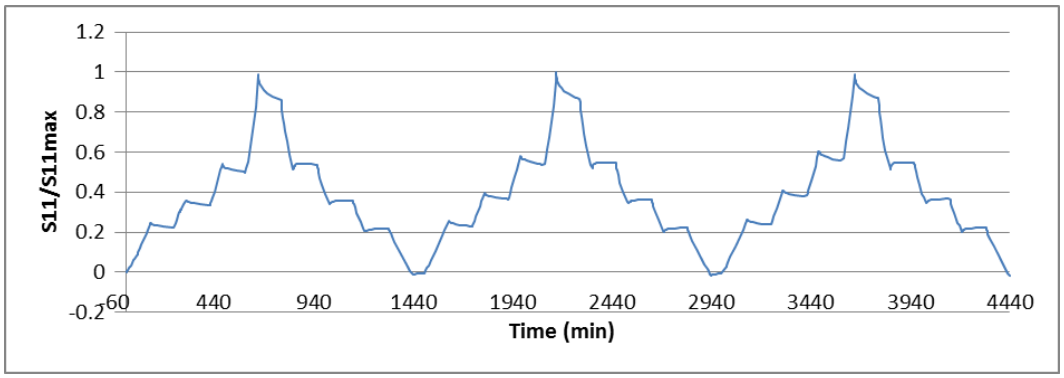

Figure 4.17. Stress history during the cyclic loading (15 deg initial debonding case).

4.2.4. Debonding Study Conclusions

In this chapter, one of the major failure cases of SRMs, namely interface debonding, was studied. In the first part of the chapter, stress analyses were performed to investigate the effect of debonding on bond-stress distribution along bond-line. It is observed that bond-stress experiences a drop 15° to 30° far from the crack tip (tip point of debonding), then increases and finally converges to a value which is the defect-free stress. This part of the study mainly focused on the effect of the material model on the defect-free stress and the decrease of the stress beyond the crack tip. As a result of the comparison, it is concluded that it is important to use nonlinear material model for correctness of the stress profile along the bond-line and time dependent viscoelastic properties together with hyperelasticity are also needed in order to properly model rate dependence of viscoelastic propellant material.

In the second part of this chapter, surface based CZM is employed for analysis of propagation of debonding along the bond-line. In surface based CZM, only traction-separation rule is added to standard contact definition of the two surfaces. Therefore, no additional modelling effort is required in implementation of this method. At the end of the analyses it is concluded that, CZM is an easy and effective method for analysis of crack propagation between two different media.

5. CONCLUSION

This study was concerned with the crack propagation analysis in nonlinear viscoelastic propellants. Firstly benchmark studies dealing with the application of crack propagation methods to some problems were performed. In the first benchmark study, conventional method based on J integral, XFEM and CZM methods were used for the crack propagation analysis of an edge cracked specimen. Comparing the methods used in this benchmark study, it is concluded that the history of the crack propagation profiles as a function of applied displacements are similar for all of the methods except for slight differences in the initiation instants. When analysis procedure is XFEM, no matter if the damage model is traction-separation or LEFM, the results are very close to each other for the analyzed problem. The most distinct results are of CZM and conventional method. From the propagation histories obtained from the analysis with different methods, it is seen that the timings of crack initiation and propagation are very close to each other. However, since the LEFM is appropriate to linear materials, throughout the thesis study, traction separation model was used.

In the second benchmark study XFEM method was applied to linear viscoelastic double-edge-cracked specimen and results were compared with the experimental and CZM results of the literature [4]. As a result of the comparison, it is concluded that crack propagation path and the reaction forces obtained with XFEM method are in a good correlation with those of the experimental results and CZM solution. Therefore, it is verified that XFEM works successfully with linear viscoelastic material model.

Upon verification of XFEM and CZM through benchmark problems, the methods were applied to analysis of SRM. Firstly bore crack problem of nonlinear viscoelastic SRMs were studied. The effects of bore cracks on stress distribution along the bondline were investigated for several crack sizes and results are compared with the related studies from literature. It can be seen from literature that bond stress experiences a drop at the angular position of the bore crack along circumference. This stress drop is used in some test based defect monitoring systems to predict the location and length

of the defect. The stress analyses for various sizes of bore cracks also revealed this stress change at the angular position of the bore crack and the relation between the bore crack length and stress change is obtained. It is therefore suggested that crack length in the motor can be predicted using the sensor readings of health monitoring systems.

The bore cracked analogue motor was then subjected to cyclic temperature loading representing the aging of the motor, and bond stress history was compared with the actual test results. This analysis shows that peak stress value decreases in the proceeding cycles as a result of the viscoelasticity effect. However, the decrease in the peak stresses is not as much as the experimental results. This is because the damaging effect was not introduced to the material model and we see only the decrease resulting from the viscoelasticity.

The propagation of bore cracks in an analog motor as a result of cyclic temperature loading was analyzed using XFEM. Firstly, for 4mm initial crack case, the amount of dissipated energy were compared with the amount of required energy calculated using J integral in order to verify FE model. It is observed that the amount of dissipated energy as a result of XFEM analysis is almost the same as the energy calculated with J integral method. Then several initial crack lengths were analyzed and the crack propagation histories were obtained. It is observed that although up to some initial crack length the crack growth increases with increasing initial crack length, after this point, crack growth decreases.

A second failure case studied for SRMs is that of interfacial debonding. Stress analyses were performed for 5°, 10°, 15°, 20° debonding angles. Bond stress profiles were compared with the results from the referenced study. It is seen that bond-stress experiences a drop from 15° to 30° far from the crack tip (tip point of debonding), then again increases and finally converges to a value which is the defect free stress. In the referenced study, analysis is performed using linear elastic material model and in the current study the analysis was repeated for nonlinear elastic and nonlinear viscoelastic material models. Comparing the stress profile along the bond line for the

material models used, it is observed that defect-free stress does not change when the nonlinearity is introduced to the material model if the stresses are in the elastic region. when the viscoelasticity is introduced to the material model, however, defect-free stress decreases. This fact strongly suggests the nonlinear viscoelastic material model in the analyses of SRMs in order to get realistic results.

Finally, crack growth analysis of initially debonded SRM was performed using CZM and crack propagation histories (increase in the debonding angle in this case) were obtained for several initial debonding angles. The relation between the initial debonding angle and the final debonging angle was obtained. Similar to bore crack case, it is observed that although up to some initial debonding angle the crack growth increases with increasing initial debonding angle, after this point, debonding decreases.

For both failure cases of SRMs, bore crack and debonding, crack propagation occurs only in the cooling part of the first cycle of cyclic loading. In the proceeding cycles, the tip stress value is decreasing because of the viscoelasticity effect and crack does not propagate. In the real situation, crack length increases as the number of cycle is increased. This situation is commonly known as fatigue of the material. In order to observe this effect in crack propagation analysis, it is required to account for evolving the damage of the materials. This fact was also concluded in the analysis of analogue motor when subjected to cyclic temperature loading representing the aging of the material (Section 3.4).

As a general conclusion to this study, it can be suggested that FEM, XFEM and CZM are effective and suitable techniques for crack initiation and propagation analysis in nonlinear viscoelatic media such as solid rocket motors. In particular, XFEM is more appropriate for bulk material crack propagation where the crack path is not known a priori. For the interface debonding problem where crack path is known, CZM provides an easy and effective methodology. Another important conclusion concerns material model selection. In order to get more realistic results from such analyses, nonlinearity and viscoelasticity should be accounted for, because the results are dependent on the material behaviour.

For future work related to this thesis study, damaging properties of the material can be introduced into the material model in order to see the effect of the cyclic loading on crack growth. This would be more realistic for cyclic loading situations. Furthermore, although this study contains some verifications based on the experimental studies from literature, the results of crack propagation analysis have to be verified with experiments with the geometry and loading conditions described here. Therefore, experimental studies for the verification of the methodologies described here can be considered as another future work related to this thesis study.

REFERENCES

1. Rice, J., "A Path Independent Integral and the Approximate Analysis of Strain Concentration by Notches and Cracks", *Journal of Applied Mechanics*, Vol. 35, pp. 379–386, 1968.

2. Song, S., G. Paulino and W. Buttlar, "A Bilinear Cohesive Zone Model Tailored for Fracture of Asphalt Concrete Considering Viscoelastic Bulk Material", *Engineering Fracture Mechanics*, Vol. 73, pp. 2829–2848, 2006.

3. Li, H. and N. Chandra, "Analysis of Crack Growth and Crack-Tip Plasticity in Ductile Materials Using Cohesive Zone Models", *International Journal of Plasticity*, Vol. 19, pp. 849–882, 2003.

4. Han, B., Y. Ju and C. Zhou, "Simulation of Crack Propagation in HTBP Propellant Using Cohesive Zone Model", *Engineering Failure Analysis*, Vol. 26, pp. 304–317, 2012.

5. Brouwer, G., F. P. Weterings and H. Keizers, "Evaluation of Ageing in Composite Propellant Grains Part 2", *43rd AIAA/ASME/SAE/ASEE Joint Propulsion Conference & Exhibit*, 2004.

6. Le, A. Q., L. Sun and T. C. Miller, "Detectability of Delaminations in Solid Rocket Motors with Embedded Stress Sensors", *Journal of Propulsion and Power*, Vol. 29 No. 2, pp. 299–304, 2013.

7. H.C. Yıldırım, Ş. Özüpek., "Structural Assessment of a Solid Propellant Rocket Motor: Effects of Aging and Damage", *Aerospace Science and Technology*, Vol. 15, pp. 635–641, 2011.

8. Miner, M., "Cumulative Damage in Fatigue", *Journal of Applied Mechanics*, Vol. 67, pp. A159–A164, 1945.

9. Vukelić, G. and J. Brnić, "J-Integral as Possible Criterion in Material Fracture Toughness Assessment", *Engineering Review*, Vol. 11, pp. 91–96, 2011.

10. Timbrell, C., R. Chandwani and G. Cook, "State of the Art in Crack Propagation", *Les Methodes de Dimensionnement en Fatigue*, 2004.

11. Mladensky, A. S. and V. I. Rizov, "Application of J-Integral in the Case of a Single Crack in Cantilever Beam", *Journal of Theoretical and Applied Mechanics*, Vol. 42, pp. 41–54, 2012.

12. Khoei, A., H. Azadi and H. Moslemi, "Modeling of Crack Propagation via an Automatic Adaptive Mesh Refinement Based on Modified Superconvergent Patch Recovery Technique", *Engineering Fracture Mechanics*, Vol. 75 No. 10, pp. 2921–2945, 2008.

13. Nishioka, T. and S. Atluri, "On the Computation of Mixed-Mode K-Factors for a Dynamically Propagating Crack, Using Path-Independent Integrals J_k", *Engineering Fracture Mechanics*, Vol. 20, pp. 193–208, 1984.

14. Abdelaziz, M. N., R. Neviere and G. Pluvinage, "Experimental Investigation of Fracture Surface Energy of a Solid Propellant Under Different Loading Rates", *Engineering Fracture Mechanics*, Vol. 31, pp. 1009–1026, 1988.

15. ASTM, *Standard Test Method for Measurement of Fracture Toughness*, E1820-01, ASTM, 2005.

16. Wong, F., "Pseudodomain Fracture Analysis of Instrumented Analog Rocket Motors", *Journal Of Spacecraft And Rockets*, Vol. 40 No. 1, pp. 92–100, 2003.

17. Brouwer, G., A. Pfiffer and L. Bancallari, "Development and Deployment of Diagnostic Prognostic Tactical Solid Rocket Motor Demonstrator", *47th AIAA/ASME/SAE/ASEE Joint Propulsion Conference & Exhibit*, 2011.

18. Miller, T. and G. Ruderman, "Modeling and Simulation of a Health Monitoring

System in an Analog Motor", *Technical Report*, 2003.

19. Wong, F., "Application of Embedded Sensor Technology to a Full-Scale Experimental Nozzleless Rocket Motor", *43rd AIAA/ASME/SAE/ASEE Joint Propulsion Conference & Exhibit*, 2007.

20. Brouwer, G. R., F. P. Weterings and H. Keizers, "Evaluation of Ageing in Composite Propellant Grains Part 2", *41st AIAA/ASME/SAE/ASEE Joint Propulsion Conference & Exhibit*, 2005.

21. Ho, S.-Y. and G. Care, "Modified Fracture Mechanics Approach in Structural Analysis of Solid Rocket Motors", *Journal Of Propulsion and Power*, Vol. 14 No. 4, pp. 409–415, 1998.

22. Liu, C., "Crack Growth Behavior in a Solid Propellant", *Engineering Fracture Mechanics*, Vol. 56 No. 1, pp. 127–135, 1997.

23. Scapery, R., "A Theory of Crack Growth in Viscoelastic Media", *Technical Report No. 2*, 1973.

24. Rao, B., "Fracture of Solid Rocket Propellant Grains", *Engineering Fracture Mechanics*, Vol. 43 No. 3, pp. 455–459, 1992.

25. Needleman, A., "A Continuum Model for Void Nucleation by Inclusion Debonding", *ASME Journal of Applied Mechanics*, Vol. 54, pp. 525–531, 1987.

26. Xu, X. and A. Needleman, "Numerical Simulations of Fast Crack Growth in Brittle Solids", *Journal of the Mechanics and Physics of Solids*, Vol. 42, pp. 1397–1434, 1994.

27. Camacho, G. and M. Ortiz, "Computational Modeling of Impact Damage in Brittle Materials", *International Journal of Solids and Structures*, Vol. 33, pp. 2899–2938, 1996.

28. Liechti, K. M. and J.-D. Wu, "Mixed-Mode, Time-Dependent Rubber/Metal Debonding", *Journal of the Mechanics and Physics of Solids*, Vol. 49, pp. 1039–1072, 2001.

29. Lucas, L. J., T. Black and D. Jones, "Evaluation of Ageing in Composite Propellant Grains Part 2", *2007 ASME Pressure Vessels and Piping Division Conference*, 2007.

30. McNary, M. J., *Implementation of the Extended Finite Element Method (XFEM) in the Abaqus Software Package*, M.S. Thesis, Georgia Institute of Technology, 2009.

31. Toolabi, M., A. Fallah, P. Baiz and L. Louca, "Dynamic Analysis of a Viscoelastic Orthotropic Cracked Body Using the Extended Finite Element Method", *Engineering Fracture Mechanics*, Vol. 109, pp. 17–32, 2013.

32. Zhang, H. H., G. Rong and L. Li, "Numerical Study on Deformations in a Cracked Viscoelastic Body with the Extended Finite Element Method", *Engineering Analysis with Boundary Elements*, Vol. 34, pp. 619–624, 2010.

33. Fries, T. and M. Baydoun, "Crack Propagation with the XFEM and a Hybrid Explicit-Implicit Crack Description", *International Journal of Numerical Methods in Engineering*, Vol. 89 No. 12, pp. 1527–1558, 2012.

34. Fries, T., N. Moës and A. Zilian, "The Extended Finite Element Method, Special Issue", *International Journal for Numerical Methods in Engineering*, Vol. 86, pp. 403–666, 2011.

35. Fries, T. and T. Belytschko, "The Extended/Generalized Finite Element Method: An Overview of the Method and Its Applications", *International Journal for Numerical Methods in Engineering*, Vol. 84, pp. 253–304, 2010.

36. Yeoh, O., "Some Forms of the Strain Energy Function for Rubber", *Rubber Chem-*

istry and Technology, Vol. 66, pp. 754–771, 1993.